Strong Amplification of ELF/VLF Signals in Space Using Neutral Gas Injections from a Satellite Rocket Engine

Paul A. Bernhardt[1], William C. Bougas[2], Michael K. Griffin[3], Chris Watson[4], Richard B. Langley[4], Andrew D. Howarth[5], H. Gordon James[5], Carl L. Siefring[1], Gareth W. Perry[6]
J. D. Huba[7], Robert Moore[8], M. B. Cohen[9] and M. Gołkowski[10]

[1]Plasma Physics Division, Naval Research Laboratory, Washington, DC
[2]Mobius Corporation, Alexandria, VA
[3]MIT Lincoln Laboratory, Lexington, MA
[4]Physics Department, University of New Brunswick, Fredericton, NB, Canada
[5]Department of Physics and Astronomy, University of Calgary, Calgary, AB, Canada
[6]New Jersey Institute of Technology, Newark, NJ 07102, USA
[7]Syntek Technologies, Fairfax, VA
[8]Department of Electrical and Computer Engineering, University of Florida, Gainesville, FL 32611-6200
[9]School of Electrical and Computer Engineering, Georgia Institute of Technology, Atlanta, Georgia, USA.
[10]Department of Electrical Engineering, University of Colorado Denver, Denver, Colorado, USA

Abstract

The first demonstration of rocket exhaust driven amplification (REDA) of whistler mode waves occurred on 26 May 2020 by transferring energy from pickup ions in a rocket exhaust plume to EM waves. The source of coherent VLF waves was the Navy NML Transmitter at 25.2 kHz located in LaMoure, North Dakota. The topside ionosphere at 480 km altitude became an amplifying medium with a 60 second firing of the Cygnus BT-4 engine. The rocket engine injected exhaust as a neutral cloud moving perpendicular to field lines that connected the NML transmitter to the VLF Radio Receiver Instrument (RRI) on e-POP/SWARM-E. Charge exchange between the ambient O^+ ions and the hypersonic water molecules in the exhaust produced H_2O^+ ions in a ring-beam velocity distribution. The 25.2 kHz VLF signal from NML was amplified by 30 dB for a period 77 seconds as observed by the RRI. Simultaneously, preexisting coherent ELF waves at 300 Hz were amplified by 50 dB during and after the Cygnus burn. Extremely strong coherent emissions and quasi-periodic bursts in the 300 to 310 Hz frequency range lasted for 200 seconds after the release. The excitation of an ELF whistler cavity may have lasted even longer, but the orbit of the SWARM-E/e-POP moved the RRI sensor away from the wave emission region. The amplified 300 Hz ELF waves may have gained even more energy by cyclotron resonance with radiation belt electrons as they were ducted between geomagnetic-conjugate hemispheres.

1. Introduction

ELF and VLF wave-generation processes in space and on the ground have been investigated for over four decades. Whistler modes that propagate in the ionosphere and magnetosphere have been excited by ground based transmitters such as SIPLE Antarctica [Helliwell, 1977], the world's high power VLF navigation transmitters [Parrot, M., et al., 2007; Ma et al., 2017; Záhlava et al., 2018; Ross et al., 2019; Meredith et al., 2019, Zhao et al, 2019b], and the high power HF facilities in Arecibo, Puerto Rico [Pradipta et al., 2007] and HAARP, Alaska [Cohen and Golkowski, 2013; Golkowski et al., 2019], or modulation of energetic electron beams on the Space Shuttle [Carlsten et al., 2019]. Three current experimental efforts

[Borovsky and Delzanno, 2019] for space-based VLF wave generation are supported in the United States by (1) the Air Force Research Laboratory with the DSX large dipole antenna operational from June 2019 to transmit VLF waves in space [Scherbarth et al., 2009], (2) the Los Alamos National Laboratory with a VLF precipitation experiment scheduled for April 2021 to launch the Beam Plasma Interactions Experiment (Beam-PIE) with electron beam generation on a sounding Rocket [Carlsten et al., 2019], and (3) the Naval Research Laboratory with an injection of 1.5 kg of barium to form hypersonic ions that are converted into lower-hybrid, whistler or magnetosonic waves [Ganguli et al., 2015, Ganguli et al., 2019]. Alternate techniques for whistler mode generation are being studied because these waves are difficult to radiate with conventional antennas where the free space wavelengths (10–1000 km) are so much longer than a practically realizable vertical monopole antenna, and the radiation efficiency is exceedingly small.

The VLF wave sources are expensive in terms of ground facility or spacecraft launch and maintenance costs. There is an on-going debate over which system has the most efficiency (Carlsten et al., 2019; Ganguli and Crabtree, 2020; Carlsten et al., 2020). Engineering design and state-of-the-art innovation for these systems adds both cost and risk to each system. In addition, each space-based device has built-in inefficiencies that increase both launch and design costs. The RF driven-antenna-in-space concept such DSX requires extremely large currents (for a loop antenna) or extremely large voltages (for dipole antennas) because it is difficult to efficiently launch VLF waves with wavelengths much larger than the physical devices. The electron beam system (Beam-PIE) requires flying a particle accelerator with only a fraction of the payload mass devoted to the electron beam itself. Finally, the ion beam chemical release of barium [Ganguli et al., 2019] uses thermite vaporization system that is typically ten-times more massive that the amount of barium gas released.

This paper presents a simple, low-cost alternate concept where the space plasma medium is converted to an amplifier (as opposed to generator) of large-amplitude VLF waves in the ionosphere. These amplified waves propagate to the magnetosphere as left-hand circularly polarized whistlers. This newly proposed technique thus converts the earth's plasma medium into a whistler mode amplifier. This work demonstrates that a large area region in space can greatly enhance the amplitude of whistler waves from either ground-based or space-based sources. This new concept for an ELF/VLF wave generation system is thus broken into three components consisting of (1) a localized ELF/VLF wave exciter or generator on the ground or in space, (2) a high-gain amplifier involving an efficient chemical injection that is distributed through the medium of space, and finally (3) the radiation belt region where further amplification can occur along with the generation of broad-band noise by interaction with radiation belt electrons. The generation component using ground and space-based transmitters has been the focus of the many previous studies described above. The distributed-region amplifier proposed here has never been previously considered by either experiment or theory. The new concept demonstrated in this paper is that neutral gas jets from a rocket motor can form a large-area amplification region in space. The process of rocket exhaust driven amplification (REDA) for coherent VLF waves employ hypersonic molecules from exhaust jets to charge exchange in the ionosphere yielding gyrating ion beams. These beams transfer energy to whistler mode waves for extremely strong amplification. The amplifier acts for a finite period (about minutes) to inject intense VLF waves along magnetic field lines into the magnetosphere. Wave amplification should accompany scattering of the radiation belt population into the loss-cone through a process called chemical-release-induced electron precipitation (cep).

For the past 11 years, the Naval Research Laboratory has conducted the Spacecraft Exhaust Ion Turbulence Experiment (SEITE I and II) aimed at providing multiple measurements of rocket engine burns leading to excitation and/or amplification of low frequency plasma waves in the space environment. The science objectives of the SEITE missions are (1) to advance physical understanding of artificial ion-ring beam generation by charge exchange with hypersonic neutral jets leading to the excitation of plasma waves, (2) to identify the electrostatic, MHD, and whistler-mode wave generation mechanisms from neutral gas injections in the ionosphere leading to enhanced noise on space sensors with comparison to ambient plasma wave noise in the plasmasphere, and (3) to evaluate dedicated rocket motor firings for launching whistler waves to study interactions with the charged particle environment in the magnetosphere. The SEITE I experiments had previously dedicated burns of the OMS engines on the Space Shuttle in conjunction with the plasma sensors (VEFI, CINDI and PLP) on the AFRL C/NOFS satellite [Bernhardt et al., 2012].

The current SEITE II experiments are employing the BT-4 engine on the Cygnus spacecraft in conjunction with the e-POP suite of instruments (RRI, GAP, and MGF) on the SWARM-E/CASSIOPE spacecraft. Maxworth, A., Glenn Hussey and Mark Golkowski [2020] have reviewed use of the radio receiver instrument (RRI) to monitor VLF waves excited by natural sources. The first SEITE II experiment showed RRI detection of enhanced finite-k_z Lower Hybrid waves during a 30-second burn from the BT-4 engine. This first experiment occurred on 22 July 2018 at a range of 50 km between Cygnus and e-POP during the OA-9E Mission [Bernhardt et al., 2020]. The OA-9E Cygnus burn did not have any effect on the 19.8 kHz VLF waves from the powerful VLF station NWC located 5630 km from the burn. The second SEITE II test was executed on 26 May 2020 during the NG-13 flight of Cygnus with the specific objective of greatly enhancing the power of existing VLF waves in the topside ionosphere. In this second case, the burn occurred directly over the NML VLF station broadcasting at 25.2 kHz and the observed wave amplification was between 20 and 30 dB. The next sections describe the first successful demonstration of rocket exhaust driven amplification (REDA) followed by supporting theory and modeling of changes in the ambient plasma environment leading to VLF wave-amplification.

2. The SEITE II Test of Rocket exhaust driven amplification during the NG-13 Cygnus Mission

The second SEITE II experiment was designed to investigate the REDA technique by firing a rocket motor on a satellite in conjunction with an existing VLF wave source on the ground. The concept for the ELF/VLF wave amplification process is based on several steps to go from a ground transmitter to a large amplitude whistler propagating into the magnetosphere. First, a monochromatic VLF, which is transmitted into space from a ground station, has been observed to change from linear into circular polarization (i.e., a whistler mode) on its path through the neutral atmosphere and into the ionosphere [Kintner et al., 1983]. The whistler mode propagates unamplified until it reaches the ion-ring distribution region setup by ion-molecule charge exchange in a rocket exhaust plume. Finally, the artificially amplified waves are guided into the radiation-belt region as whistler mode for further intensification by wave-particle interactions. A diagram of the concept is given in Figure 1.

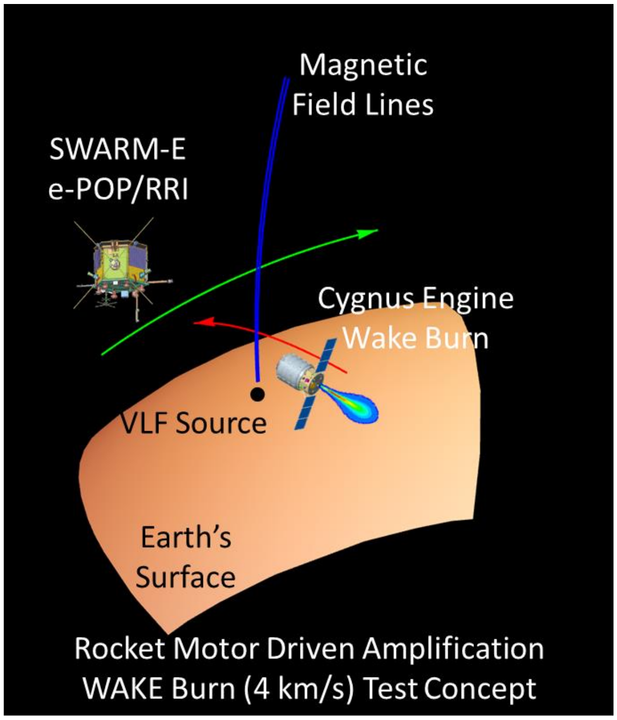

Figure 1. Detailed configuration of the NG-13 Cygnus engine operation to yield the injection velocities perpendicular to a (blue) magnetic field line with wake burn. The Cygnus spacecraft is moving horizontally along the red trajectory. The injection speed determines the kinetic energy of the ions created by the charge exchange process in the ionosphere. The plasma wave observations with the RRI on SWARM-E (green trajectory) will be made during the REDA tests with enough energy to form a ring-beam ion velocity distribution that can promote EM wave amplification.

This test of REDA used the BT-4 on the Cygnus spacecraft that serviced the ISS during the NG-13 Mission. The single BT-4 thruster produces 450 N of thrust by burning a mixture of NTO and Hydrazine (N_2O_4 (97%) + NO (3%) + N_2H_4). This combustion yields a number of molecular exhaust products according to the reaction

$$N_2O_4 + 2N_2H_4 \rightarrow 4H_2O^* + 3N_2^* \; . \qquad (1)$$

The BT-4 rocket yields an exhaust velocity of 3185 m/s with a flow rate of 0.147 kg/s.

The NC-13 Cygnus was launched on 15 February 2020 and reentered the Earth’s atmosphere on 29 May 2020. After Cygnus undocked from the Space Station on 11 May 2020, it went into a free-flyer mode performing a number of experiments including the NRL SEITE II burn starting on 26 May 2020 at 00:13:20 with a 60-second burn of the BT-4 engine. The burn end time (00:14:20 UT) was chosen to occur when the exhaust source (Cygnus) was between a ground VLF transmitter (NML) and the plasma sensor satellite (e-POP) on the same magnetic line (Figure 2). This experiment geometry allowed amplification of the whistler mode waves generated by the 25.2 kHz radio emissions from NML US Navy Transmitter at La Moure, North Dakota that couple through the bottomside ionosphere to reach the Cygnus orbit.

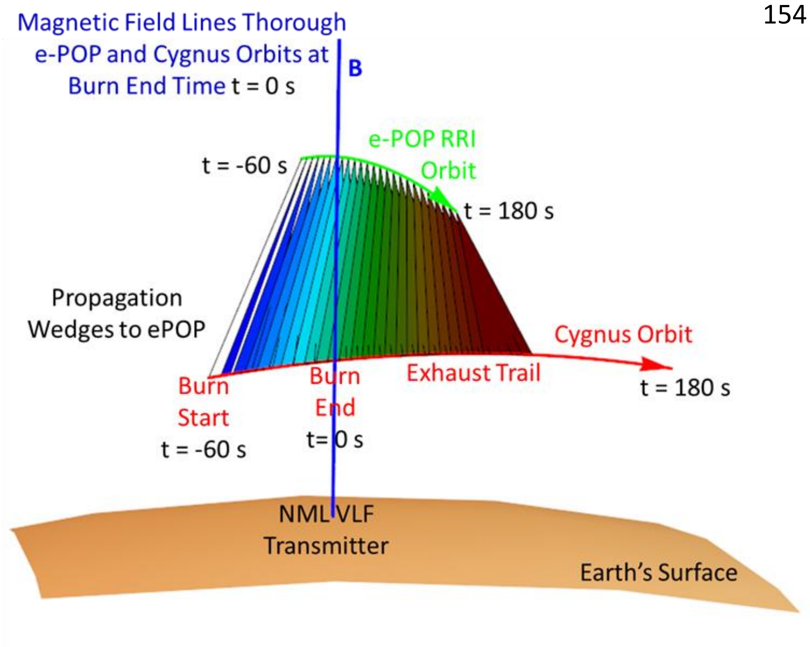

Figure 2. Cygnus-e-POP burn on 26 May 2020 for a magnetic field line conjunction with the NML VLF transmitter on the ground. The amplified emissions from the exhaust trail regions propagate in the triangles to the e-POP Radio Receiver Instrument at a higher altitude orbit. The 60 s BT-4 Burn was terminated at 00:14:26 UT when the Cygnus orbit contacted the magnetic field line (**B**) that crossed the orbit e-POP 20 seconds later. At that time, the altitudes of Cygnus and e-POP were 481 km and 1063 km, respectively.

The NML transmitter radiates continuously with 250 to 500 kW power and a 300 Hz FSK modulation for communications to submerged submarines. The 25.2 kHz VLF waves must first pass through the region of BT-4 exhaust cloud to reach the VLF receiver of e-POP. For this experiment, the e-POP/RRI was observing wave emissions in the 10 Hz to 35 kHz frequency range. The RRI instrument is connected to a pair of 6-m dipoles denoted as channels A and B [James, 2006; James et al. 2015]. The dipoles are located on the ram face of the spacecraft at 45 degrees to the orbit plane. The Cygnus spacecraft was moving at 7.3 km/s while the e-POP orbit speed was 7.7 km/s, both nearly perpendicular to the magnetic field line. The BT-4 nozzle was pointed in the ram direction of the Cygnus orbit for a posigrade burn that injects the exhaust with a speed of 7.3 – 3.1 = 4.2 km/s. This orientation placed the exhaust cloud moving across the magnetic field line at the time of intersection by the e-POP instruments.

The NG-13 Cygnus burn occurred at an altitude chosen to have sufficient ambient O^+ ions to charge exchange with the injected wave vapor and for geographic location above a ground VLF transmitter. The locations of the two satellites in both geographic and geomagnetic coordinates are given in **Table I**. The end of the Cygnus burn was located near a single magnetic field line containing the e-POP orbit and was almost directly above the 25.3 kHz VLF transmitter located at 46.366° N Latitude and -98.3367° E Longitude. **Table** I also provides the in situ values of electron densities based on GPS TEC measurements and models as explained in Section 5.

Table I. Geographic, Geomagnetic and Plasma Parameters of the Cygnus and e-POP/SWARM-E Satellites for the NG-13 Burn during Second SEITE II Experiment

Parameter	Burn Start	Burn End
Time (H:M:S GMT)	00:13:20	00:14:20
Cygnus Altitude (km)	480.3	480.9
Cygnus Longitude (°E)	-102.7	-98.5
Cygnus Latitude (°N)	41.7	43.8
Cygnus L Shell	2.39	2.61
Cygnus Magnetic Longitude (°E)	-27.1	-22.6
Cygnus N_e (10^4 cm^{-3})	8.3	8.3
ePOP Altitude (km)	1040.4	1063.9
ePOP Longitude (°E)	-99.7	-98.8
ePOP Latitude (°N)	47.3	44.1
ePOP L Shell	3.31	2.85
ePOP Magnetic Longitude (°E)	-24.6	-23.6
ePOP N_e (10^4 cm^{-3})	0.82	0.77

The proposed mechanism for VLF wave amplification is to have Cygnus inject exhaust perpendicular to B and produce charge exchange with the ambient oxygen ions with the reactions

$$H_2O^* + O^+ \rightarrow H_2O^{+*} + O, N_2^* + O^+ \rightarrow NO^{+*} + N \quad (2)$$

The resulting pickup ions form into a ring-beam distribution with perpendicular ion motion near 4 km/s. The ring-beam distribution, previously measured with incoherent scatter radar from a Space Shuttle OMS burn by Bernhardt and Sulzer [2004], can excite a variety of plasma oscillations including Lower Hybrid waves and Fast MHD/Alfven Waves. The Lower Hybrid wave may act as a pump for Parametric Amplification of the whistler mode provided by the ground NML transmitter. This amplified wave then propagates along the magnetic field line as a whistler mode to be observed 580 km higher in altitude by the RRI electric field sensors. Other mechanisms for amplification of whistler waves by interaction with energetic electrons have be proposed by Lee and Crawford [1970]. With these parametric or electron-interaction amplification processes in mind, the SEITE II/REDA experiment was conducted employing orbit planning and burn execution by Northrup Grumman, NASA and MIT/LL during the NG-13 flight of Cygnus. Besides the RRI on e-POP, the magnetometer (MGF) observed magnetic field changes and the GPS occultation (GAP-O) and Attitude (GAP-A) receivers obtained data on the total electron content (TEC) to 6 GPS satellites.

The geometry for the NG-13 SEITE experiment is shown in Figure 2. VLF signals generated on the ground by the NML transmitter become amplified as they passed through the exhaust trail along the Cygnus orbit. To reach the position of the VLF receiver (RRI) on the e-POP orbit, the waves must travel along the colored triangular wedges shown in the figure. For whistler mode, this propagation from the pickup-ion trail to receiver occurs if the line-of-site paths make an angle of 19.6 degrees or less with the magnetic field lines

[Storey, 1953; Swanson, 1989]. For the NG-13 Cygnus flight geometry, this condition lasts for about 60 seconds after the burn termination time. In summary, detection of amplified VLF waves by the RRI on e-POP require (1) energy transfer from the gyrating pickup ions in the Cygnus exhaust trail, and (2) approximate alignment of the propagation paths with the earth’s magnetic field lines.

3. RRI Measurements of the NG-13 VLF Wave Amplification for SEITE II

The VLF waves recorded by the RRI on e-POP showed extremely strong amplification of the 25.2 kHz transmission (Figure 3.) along with another ambient signal at 300 Hz. In addition, the low frequency 300 Hz wave introduced harmonics in the plasma wave receiver data. Figure 3 shows an overall view of the ELF and VLF spectrum from the A and B channels of the RRI of e-POP. Starting 10 seconds after the initiation of the burn, the signals from NML were amplified for a period of about two minutes. Multiple harmonic sidebands with separations near 600 Hz occurred around the 25.2 MHz VLF carrier. This region is labeled Amplified VLF in Figures 3a and 3b for channels A and B, respectively. The ambient strong plasma wave emission (SPWE), discovered in 2018 by Bernhardt et al. [2020], was also amplified in channel A. Finally, ELF wave emissions with odd harmonics of 300 Hz are observed in channels A and B. The VLF wave signal powers return to their pre-event levels at about 3 minutes after the end of the burn. In the discussions of the data analysis and the model studies, time will be referenced to the termination of the burn, which is also the time for Cygnus to be located on the common field line between Cygnus and e-POP (Figure 2).

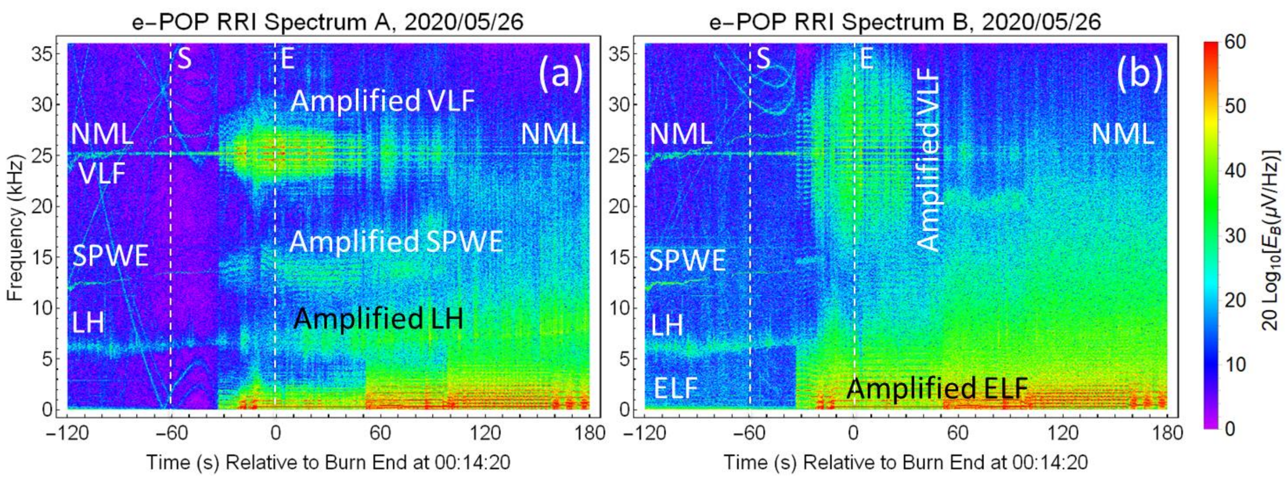

Figure 3. Channels A (left) and B (right) of the radio receiver instrument (RRI) on e-POP during the fly over of the 25.2 kHz VLF NML transmitter in North Dakota. A dedicated 60-second burn of the Cygnus BT-4 thruster occurred during the times labeled as S (start) and E (end). Observational data will be referenced to time (t) relative to the termination time (00:14:22 GMT) of the burn.

Each of the burn-induced features of the measured ELF/VLF spectra will be discussed separately. The 20 to 30 dB VLF amplification at 25.2 kHz shows the strongest correlation with both ignition and shut-down of the Cygnus engine. As such, this amplification alone demonstrates success of the rocket motor driven acceleration (REDA) concept. A discussion on amplification of the SPWE will be postponed to the future because the source and nature of the SPWE are unknown with speculation that it is related to finite k_z lower hybrid waves [Bernhardt et al., 2020]. The amplified lower hybrid (LH) frequencies will not be discussed here. Major focus will be devoted to the 50 dB amplification of 300 Hz ELF waves that, after the initial amplification by the Cygnus burn, excited an enhancement-duct resonator that extended through the radiation belts for further amplification.

The Cygnus burn established an amplifying plasma environment producing a 1000-fold power gain for the VLF signal from NML as measured by the e-POP RRI. The 77 second portion of the amplification labeled REDA in Figure 4 started at 00:13:45, 35 seconds after the start of the burn, and ended at 00:15:12, 52 seconds after the end of the burn. This is a period of favorable propagation for whistler mode between the exhaust trail and the RRI as illustrated in Figure 2. Amplification is observed in exactly the region predicted for whistler propagation from the Cygnus exhaust trail to e-POP based on the favorable propagation angle relative to the field line vector **B**.

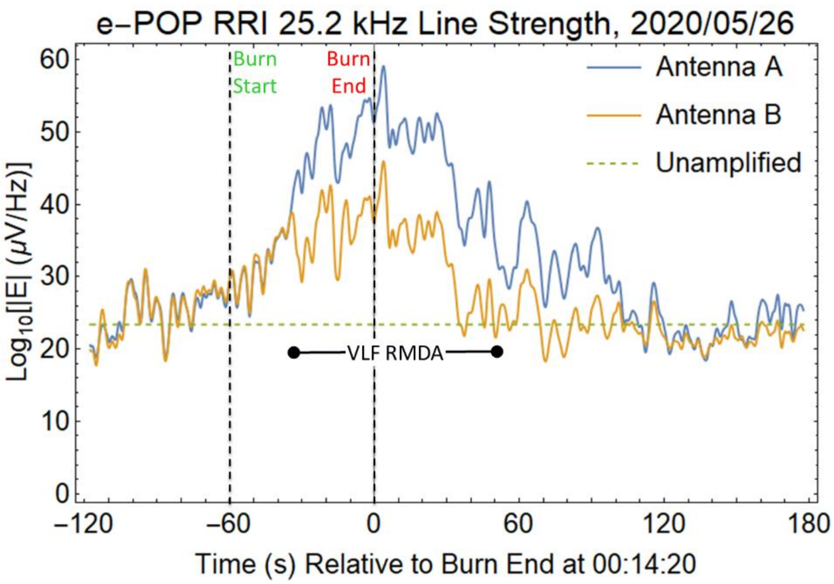

Figure 4. The measured NML carrier strength showing strong VLF amplification by whistler mode propagation through the modified ionosphere during and after the 60 second BT-4 burn of the Cygnus motor. The period of strong REDA lasted for 76 seconds.

The observed amplification is remarkable because of the enormous VLF power gain provided by the plasma region energized by fast ions in the Cygnus exhaust plume. The measured gain of the REDA system is large, but different, for each the two channels, being 34 dB for channel A and 22 dB for channel B. The 60 second burn of the BT-4 motor on Cygnus provided 9 kg of exhaust distributed over a horizontal distance of 432 km in 60 seconds. The kinetic energy of this injection is 78 M Joules or a power or P_{Burn} = 1.3 MWatts for 60 seconds. Thus, a large amount of kinetic energy is input into the ionospheric plasma system to be available for amplifying whistler mode waves. After amplification of the signal from the 500 kW NML transmitter, the measured signal strength is equivalent to a 60-second transmission from a 500 MW ground transmitter. This is important because the estimated ELF and VLF power that can reach the upper atmosphere from ground based systems is on the usually less than 1 Watt, up to hundreds of Watts at best [Cohen and Golkowski, 2013].

The estimated power in the amplified waves is given by $P_{WT} = \frac{|E|^2 \Delta f^2}{\eta_0 n_W A_{RRI}} A_{Exhaust} = 8.5\ \mathrm{kW}$ where E is the electric field in Figure 4, Δf = 10 Hz is the spectral analysis frequency bin, η_0 = 377 Ohms, n_W = 32 is the Whistler mode refractive index, A_{RRI} = 36 m^2 is the RRI Antenna area, and $A_{Exhaust}$ = 10^{10} m^2 is the amplification area of the Cygnus burn region. The REDA efficiency is for this experiment estimated to be P_{WT}/P_{Burn} = 0.5 %.

This efficient estimate neglects the angular spreading for waves travelling between Cygnus and RRI. If the waves are confined to a 19.6 degree cone for the length of 582 km long propagation paths, the projected area of the exhaust cloud grows to the has been neglected for the whistler mode. If the stimulated whistler waves radiate inside a 19.6-degree propagation cone, the projected exhaust grows to 5 x 10^{11} m^2. With waves spread over this area, the total power grows to 400 kW and the energization efficiency using the measured electric field strength increases to 25%. This number will be refined with future propagation studies using a three-dimensional model of the chemical release.

The temporal changes in received 25.2 kHz wave power correlate well with the burn before, during, and after the burn event but there is about 10 dB difference between A and B in the amplification phase (Figure 4). Before the experiment, it was expected that the power levels on those two channels would be the same because those antennas are located at an angle of ±45 Degrees to the plane containing the e-POP orbit and the earth's magnetic field. Also, note that the sideband generation is significantly different on the two RRI channels. This effect is the result of signal saturation of the RRI preamplifier and it will be discussed in more detail later.

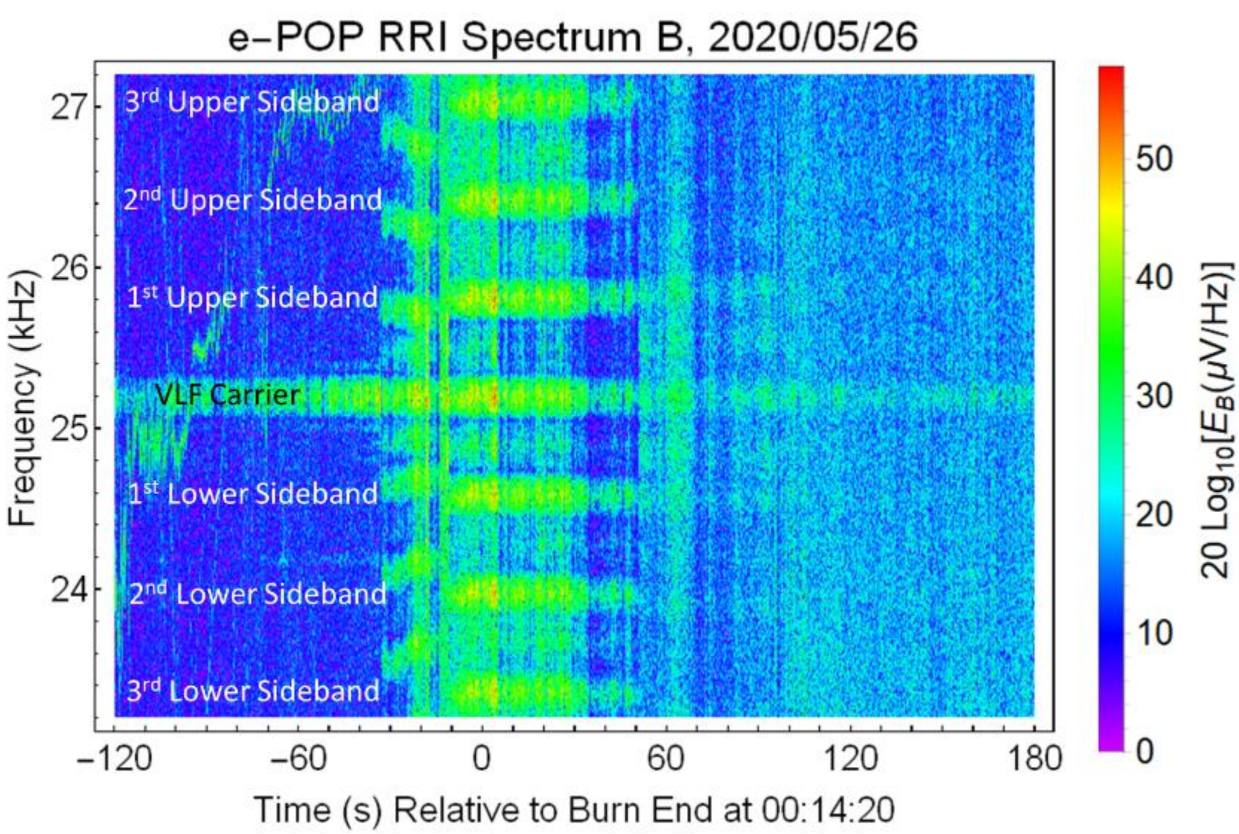

Figure 5. Symmetric sidebands around the 25.2 kHz modulated carrier signal from NML. The RRI channels A and B contain sidebands separated by 600 Hz starting at 30 seconds after the burn starts at (00:13:20) and lasts for 60 seconds after the burn ends. These sidebands are attributed to saturation of the RRI preamplifier by a separate strongly amplified signal near 300 Hz seen in the spectrum of Figure 6.

The e-POP RRI observations show a 25.2 kHz transmission from NML that is modulated with multiple sidebands separated by 600 Hz that extend from the carrier by multiples of ±4 for channel A and ±15 for channel B (Figures 3 and 5). The upper and lower sidebands with power levels close to the center carrier have the same bandwidth as the NML carrier. The Channel A sidebands extend out ± 2 kHz from the carrier while the sampled electric fields on Channel B extend out to ± 10 kHz with about 10 dB drop in signal strength. These sidebands are not from nonlinearities in the plasma but, based on spacecraft engineering analysis, are from nonlinear saturation of the preamps used in the e-POP RRI. These sidebands are the result of overdriving the input preamplifier for the RRI by a second, ELF signal at 300 Hz that is even more strongly amplified in the active plasma cloud region of by the Cygnus burn.

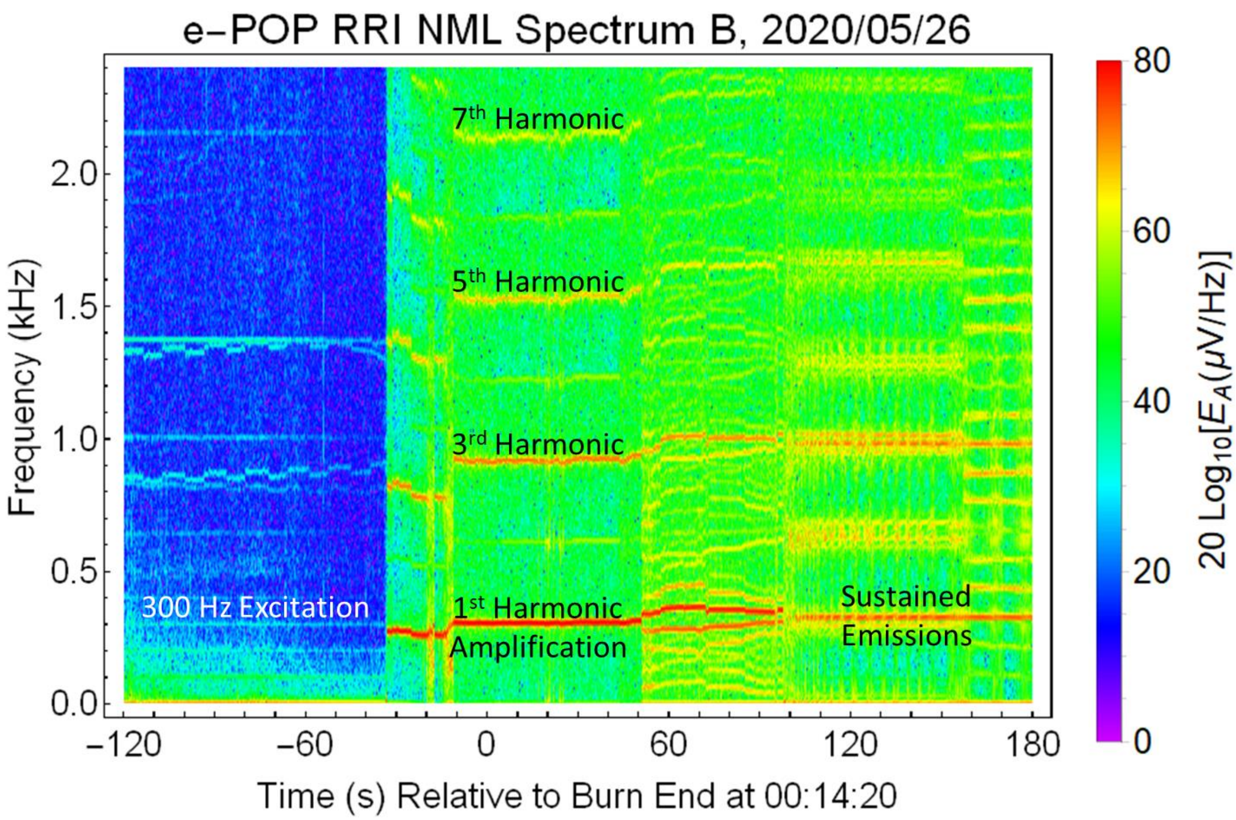

Figure 6. Ambient harmonics of 100 Hz and other ELF signals are present in the RRI spectrum before the 60-second Cygnus burn. The ELF radio emissions, associated with harmonics of 100 Hz in the spectrum, excite a strongly amplified wave near 300 Hz labeled 1st Harmonic. Remnants of the amplified signal evolving into sustained split and burst modes last for more than 180 seconds after the termination of the burn. The odd harmonics at 900, 1500, and 2100 Hz result from overdriving the preamplifier in the Radio Receiver Instrument that recorded the data.

The amplification of the ELF wave at 300 Hz is much larger than the amplification for the 25.2 kHz VLF wave. The ambient 300 Hz signal has a power level of about 30 dBμV/Hz starting at 00:13:56, 24 seconds before the end of the burn (Figure 6). The active plasma medium then enhances the signal power by 50 dB to 80 dBμV/Hz maintaining a constant power for about 74 seconds. The 3rd, 5th, and 7th harmonics that are very prominent in the spectrum are attributed to overdriving the RRL preamp. The sustained emissions and bursts near 300 Hz 50 to 160 seconds after the end of the burn are produced by excitation of a magnetic field aligned resonator for whistler mode that extends between hemispheres.

The environmentally amplified 300 Hz ELF signals couple into the RRI antennas and drive the input preamps of the RRI into compression. This converts the sinusoidal waveform of the plasma wave into a symmetrical square wave that is digitized by the A/D converter in the RRI. The distortion of the waveform by the preamp is responsible for the odd harmonics at 300 Hz and the sidebands at 25.2 kHz.

The preamp saturation with the 300 Hz signal induces sidebands into the 25.2 kHz that are separated by 600 Hz. The preamp saturation occurs twice every 300 Hz cycle. This is equivalent to modulating the 25.2 kHz by multiplying a 600 Hz asymmetric pulse wave that transitions from full ON to OFF. In frequency space, this represents a convolution of the 25.2 kHz with the 600 Hz harmonics in the spectrum of the multiplication pulse. Analysis of the overdriven preamp indicates that the 300 Hz signal is compressed by 3 dB and the 25.2 Hz signal is compressed by 7 dB. All of the harmonics or harmonics modulations for both signals are instrumental and have no origin in the excited plasma medium.

The amplitude of the 300 Hz ELF signal at e-POP is isolated using a 10 Hz wide tracking filter (Figure 7). The ambient, unamplified 300 Hz wave is on the order of 30 dBμV/Hz in channel B until it is rapidly enhanced to 80 dBμV/Hz by REDA. This level remains constant for 50 seconds after the Cygnus engine shutoff. This is the same period of 30 dB amplification for the 25.2 kHz VLF signal shown in Figure 7. Unlike the VLF frequency, the 300 ELF continues at elevate power past the REDA period. At this later time, the ELF wave drifts in frequency, is split into several sidebands and enters into a sustained/burst mode as labeled in Figures 6 and 7.

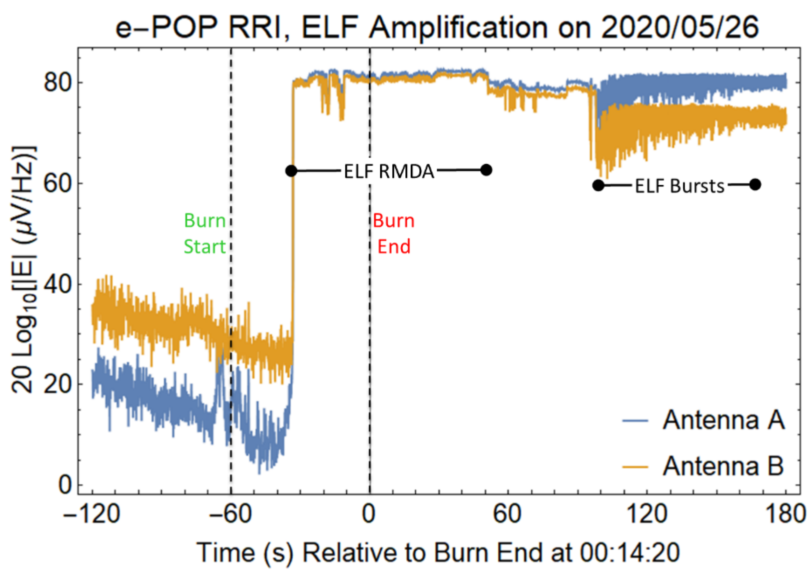

Figure 7. Amplification of the 300 Hz whistler wave by the plasma medium driven with a chemical injection of molecular rocket exhaust. The sudden increase in ELF signals on both channels A and B of the RRI occurs 28 seconds after the start of the rocket motor and it stays for more than 50 seconds after the rocket engine stops.

The 300 Hz wave spectra shown in Figure 6 can be broken into 3 phases. Between times of -35 seconds and +52 seconds, the amplified ELF is monochromatic with a constant strength near 80 dBμV/Hz. This is the same period for amplification of the 25.2 kHz VLF mode. This period is the direct rocket exhaust driven amplification (REDA) period. From 52 to 98 seconds after burn end, the ELF (300 Hz) spectrum breaks into at least 4 frequency sidebands around 300 Hz. From 98 to 160 seconds, the 300 Hz signal coalesces to one frequency with periodic noise bursts that resemble those observed with DEMETER by Hayosh et al. [2015] in conjunction with electron precipitation. A high-resolution spectrogram of the bursts is shown in Figure 8. These large amplitude (6 mV/Hz) signals at 330 Hz have a time separation of about 0.4 s.

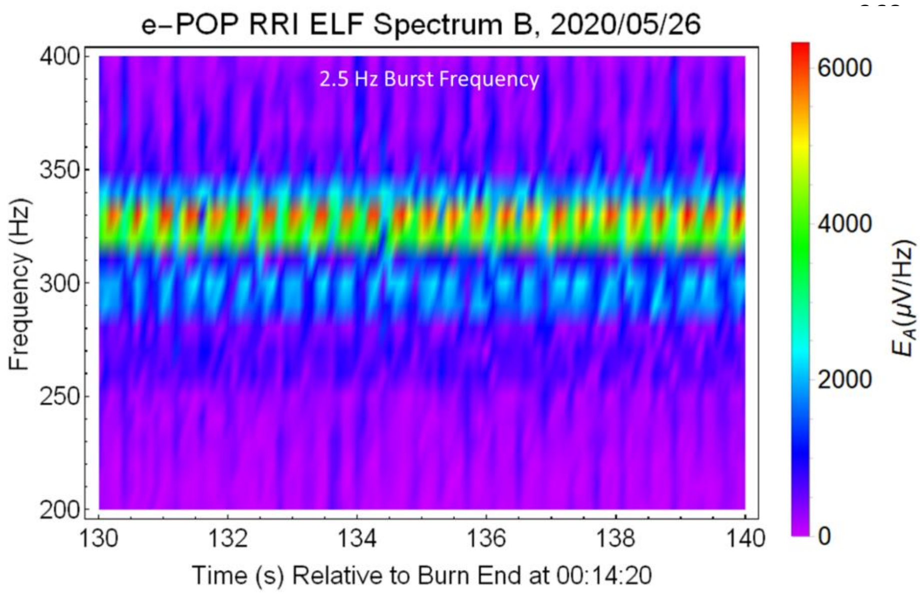

Figure 8. Cygnus burn triggered ELF noise bursts associated with late time propagation of multi-hop, ducted whistler waves following the burn of the Cygnus engine on an L = 2.8 field line.

Table II. Cygnus-ePOP Burn and Rocket exhaust driven amplification (REDA) Observation Times

Time (H:M:S GMT)	00:13:20	00:14:20	00:13:20	00:13:20	00:13:20	00:13:20
Time After Burn Start	0	25 s	60 s	112 s	158 s	220 s
Time Offset from Burn End	-60 s	-35 s	0 s	52 s	98 s	160 s
Cygnus Event	BT-4 ON		BT-4 OFF			
300-330 Hz ELF Event		RMDA Start		300 Hz Lock Lost	330 Hz Lock Burst Start	330 Hz Burst Stop
25.2 kHz VLF Event		RMDA Start		RMDA Stop		
GPS TEC Reduction	0 TECU	0 TECU	0.17 TECU	0.22 TECU	0.20 TECU	0.15 TECU

The timing for the VLF and ELF events is summarized in Table II. Both the ELF and VLF signals are amplified for the same time periods relative to the Cygnus engine burn ignition and termination. The ELF emissions after amplification continue for another 108 seconds as frequency-drifting, narrowband signals and quasi-periodic bursts with 400 ms periods. The GPS TEC reductions associated with the recombination of the molecular pickup ions start just after the end of the burn as discussed in Section 5.

The VLF and ELF electric fields recorded by the RRI show (1) amplified signals that are easily observed in the data even though the RRI preamp is over driven at ELF, (2) that the preamp compression of the 300 Hz and 25.2 kHz carriers are estimated to be 3 and 7 dB respectively, and (3) that the neutral injection technique yields a plasma medium with 50 dB gain for 300 Hz and 30 dB gain for 25.2 kHz. A water vapor and molecular nitrogen injection at 4.2 km/s perpendicular to **B** will charge exchange with the ambient atomic oxygen ions to produce an ion-ring distribution. These measurements give convincing evidence and demonstrate that REDA greatly enhances both ELF and VLF whistler mode waves. In the following sections, the other e-POP sensors and a model of the orbital chemical release give more weight to this interpretation of the NG-13 REDA experiment during SEITE II.

4. Computational Model of the Cygnus Exhaust Release and Interactions in the Ionosphere

The first step in the analysis of the NG-13 Cygnus burn is to model the injected exhaust cloud and subsequent charge exchange in the background ionosphere. The neutral gas expansion from a rocket motor can be described by continuum, kinetic, or particle models depending on the injection altitude and mean free path. The exhaust from Cygnus was released at 480 km altitude at a supersonic speed of 4.1 km/s relative to the background atmosphere, which has a horizontal mean free path of 460 km. Under these conditions, the neutral expansion can be described by the following equations for collisionless expansion into a vacuum

$$N_n(R,\theta,\phi,t) \approx \frac{N_{D0}}{8\pi R^2 v_S}\Phi_\theta(\theta)\left\{\text{erf}\left[\frac{R - t v_S}{\sqrt{2} R v_m / v_S}\right] - \text{erf}\left[\frac{R-(t-\min[t,t_e])v_S}{\sqrt{2} R v_m / v_S}\right]\right\}$$

$$\text{with } \Phi_\theta(\theta) = \frac{\text{erf}\left(\dfrac{\theta+\theta_0}{\Delta\theta}\right) - \text{erf}\left(\dfrac{\theta-\theta_0}{\Delta\theta}\right)}{\exp\left(-\dfrac{\Delta\theta^2}{4}\right)\cos\theta_0 - \text{erf}\left(\dfrac{\theta_0}{\Delta\theta}\right)} \quad (4)$$

where R, θ, ϕ are spherical coordinates, $N_{D0} = 3.94 \times 10^{24}\ s^{-1}$ is the molecular flow rate, V_S 3.2 km/s is the exhaust velocity, v_m = 0.1 km/s is the thermal speed, $\Delta\theta$ = 30 degrees is the plume angle and t_e = 60 seconds is the duration of the engine burn. The number ratio of water molecules to nitrogen molecules is 4:3. The simulation of the injection moves the source at 7.3 km/s with the nozzle pointed in the ram/posigrade direction. More details on the modeling of molecular exhaust flow are provided by Bernhardt [1979], Kaplan and Bernhardt [2010], and Bernhardt et al. [2012].

The Cygnus engine is operated for 60 seconds while moving horizontally at 7.3 km/s. The BT-4 engine operated while pointed in the ram direction relative to the orbit of the satellite. In the neutral exhaust model, the orbit is along the z-axis and the exhaust plume expands to form a cone in cylindrical coordinates relative to the radial (r) and axial (z) directions. The plume model neglects the compensating effects of the curvature of the orbit and the force of gravity. Figure 9 shows the neutral density at four times (0.5, 1, 2 and 3 minutes) after the start of the burn. Charge exchange with the water vapor and atomic oxygen ions produce supersonic H_2O^+ pickup ions that drive the VLF wave amplification process. The expanding cloud of water vapor is dense enough to yield energetic pickup ions several minutes after the rocket motor stops (Figure 9).

The exhaust expansion model assumes that all the exhaust material vaporizes. Yu. V. Platova, A. I. Semenovb, and B. P. Filippova [2011] have considered the condensation process of water vapors in the exhaust plume of a rocket engine in the upper atmosphere. After formation, the ice particles evaporation by heating during the release of latent heat of condensation, radiative heating, and energy losses to emission. The re-evaporation process produces hypersonic water molecules down-stream from the injection point and will increase the size of the wave amplification region. Re-evaporation may be responsible for the extend duration of the VLF amplification after the Cygnus motor shuts off.

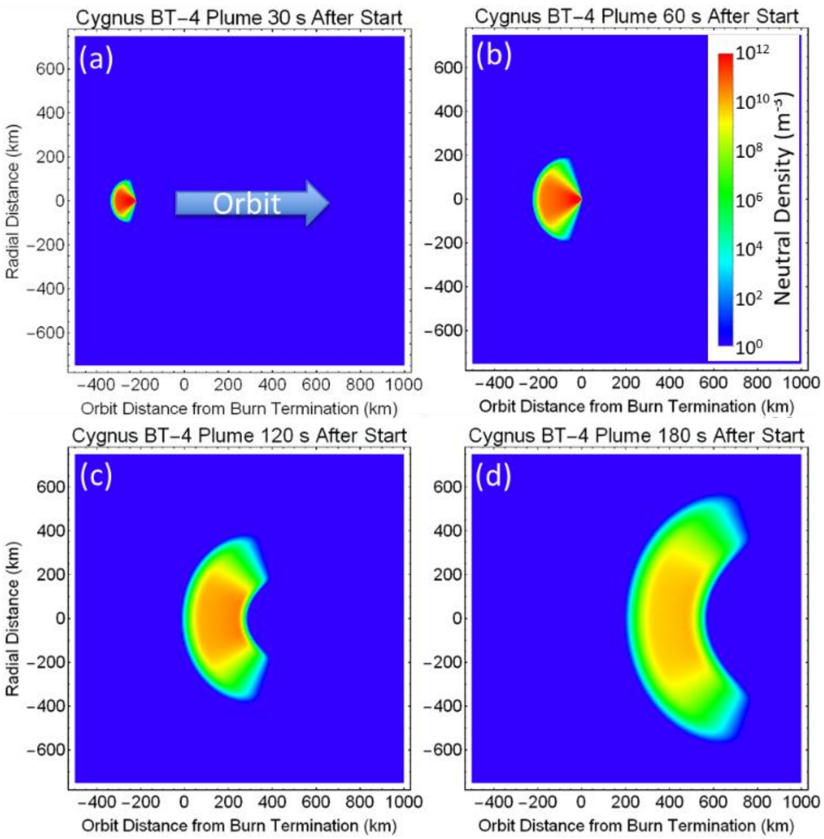

Figure 9. Neutral (H_2O plus N_2) densities along the Cygnus orbit for a 60 second burn of the BT-4 motor when the motor is firing at (a) t = 30 and (b) 60 s. After the motor shuts off, the plume becomes an expanding shell at (c) t = 120 s and (d) t = 180 s. The length of the plume along the orbit axis is identical to the length of the exhaust trail segments in Figure 2.

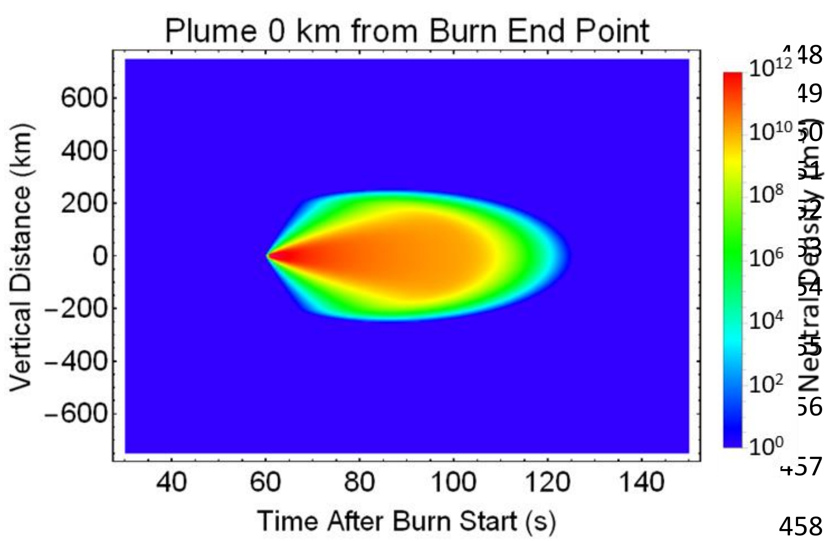

Figure 10. Exhaust molecule density at the L = 2.61 field line containing the termination point of the Cygnus engine burn. The vertical distance is taken to be the z-coordinate along the magnetic field line.

Water ions produced at high speed become attached to magnetic field lines by moving in spiral orbits. The density of the exhaust cloud on the field line at the termination point of the burn has the temporal history illustrated in Figure 10. This cloud reacts with the ambient O^+ and e^- species to give the product ions and neutrals shown in equations (2) and (3). All the times, t, is relative to the burn start even though the observations are presented relative to burn end. The cloud will be exciting the ion-ring distributions well after t = 100 seconds (or 40 seconds after the end of the 60-s burn). This explains the similar duration for VLF wave amplification in the measured data of Figure 4.

The production of whistler mode amplification Ions requires hypersonic flow of water ions. The ion plasma expansion is computed using one-dimensional solution for flow along a magnetic field line **B** in the z-direction. The ionized species are dispersed by plasma transport described by the equations of continuity

$$\begin{aligned}\frac{\partial n_1}{\partial t}+\frac{\partial}{\partial z}(n_1 v_{1z}) &= -k_{1E} n_1 n_E \\ \frac{\partial n_2}{\partial t}+\frac{\partial}{\partial z}(n_2 v_{2z}) &= k_{1E} n_1 n_E - k_{e2} n_2 n_e\end{aligned} \qquad (4)$$

and the equations of motion with an ambipolar electric-field setup by the electrons

$$\begin{aligned}\frac{\partial v_{1z}}{\partial t}+\frac{1}{2}\frac{\partial v_{1z}^2}{\partial z} &= -\frac{1}{n_1}\frac{\partial n_1}{\partial z}v_{T1}^2-\frac{1}{n_e}\frac{\partial n_e}{\partial z}v_{Te1}^2-g_0\sin I-\nu_{1n}v_{1z}-\eta_{12}n_2(v_{1z}-v_{2z}) \\ \frac{\partial v_{2z}}{\partial t}+\frac{1}{2}\frac{\partial v_{2z}^2}{\partial z} &= -\frac{1}{n_2}\frac{\partial n_2}{\partial z}v_{T2}^2-\frac{1}{n_e}\frac{\partial n_e}{\partial z}v_{Te2}^2-g_0\sin I-\nu_{2n}v_{2z}-\eta_{12}n_1(v_{2z}-v_{1z})\end{aligned} \qquad (5)$$

where the subscripts 1 and 2 refer to the respective ions O^+ and H_2O^+, k_{1E} = 2.49 x 10^{-15} m^3/s is the charge exchange reaction rate between O^+ and H_2O based on ion-neutral cross sections provide by Li et al. [1995], k_{e2} = 10^{-12} provided by Banks and Kockarts [1973], V_T is the thermal ion speed, g_0 is gravitational acceleration, $\nu_{1n} = \nu_{1n}$ = 0.0038 s^{-1} is the ion neutral collision frequency which based on the neutral MSIS Model density at the injection altitude and η_{12} = 9.7 x 10^{-14} $m^3/2$ is the momentum transfer factor for ion-ion collisions from Banks and Kockarts [1973]. These equations are solved by the NRL SAMI2 and 3 models along with the energy equation for the ions and electrons [Huba, Joyce and Fedder, 2000]. Here, these equations are solved without ion inertia and advection, neglecting gravity, and excluding the effects of the N_2 molecule because of its slow reaction rate (10^{-18} m^3/s) with O^+.

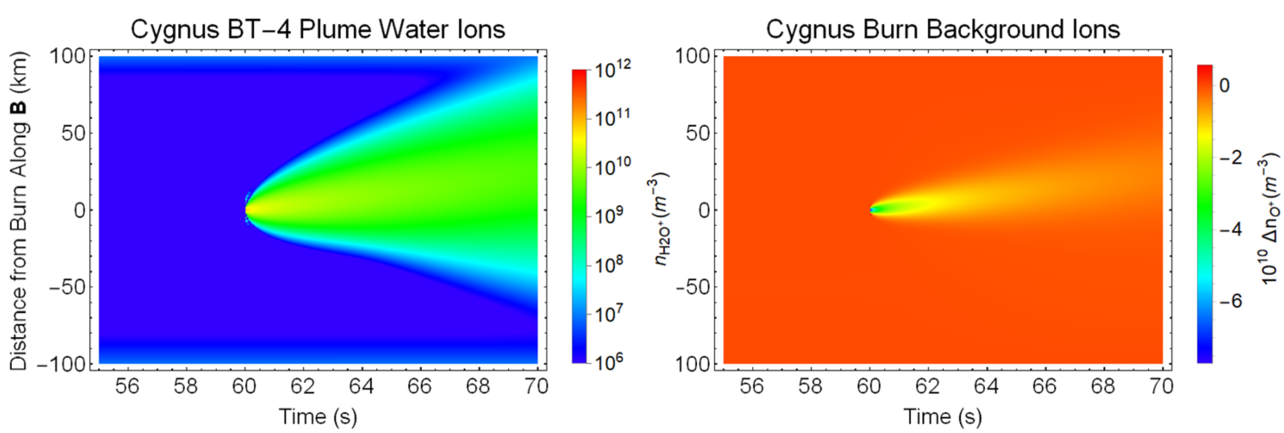

Figure 11. Estimation of the pickup ion and ambient ion densities from solutions of continuity and momentum equations with charge exchange chemistry and ion-electron recombination chemistry. The origin of the distance axis is 480.9 km in altitude and the field line is located at the end of the burn. The time is relative to the start of the 60-s burn.

The results of this simulation for the ion changes on the field line located at the end to the burn are shown in Figure 11. The neutral density release presented in Figure 10 is used to react with the oxygen ions in the ionosphere at 480 km altitude. The injected neutrals produce high-speed water ions that diffuse along magnetic field lines. The oxygen ion hole produced by ion-molecule charge exchange and are filled-in by field-aligned diffusion. The computed ion expansion rate is supersonic so the inertial and advection terms in the momentum equations need to be included in future, more accurate solutions. Acoustic shock flow is expected to slow the expansion of water ions along the magnetic field lines.

5. Background Plasma Conditions Observed with the GPS Attitude and Position (GAP) sensor and Magnetic Field (MGF) instrument on e-POP.

Validation of the formation of hypersonic molecular ions is provided by measurements of the recombination of these ions with electrons. This measurement is made with total electron content for GPS signals passing through the modified ionosphere. The GPS Attitude and Position (GAP) sensors on SWARM-E/e-POP are comprised of three working antennas located on the top of the SWARM-E/CASSIOPE satellite and on the one antenna on the anti-RAM face of the satellite. These antennas feed five separate GPS receivers for determination of total electron content (TEC) to any GPS satellite in view of the e-POP sensor.

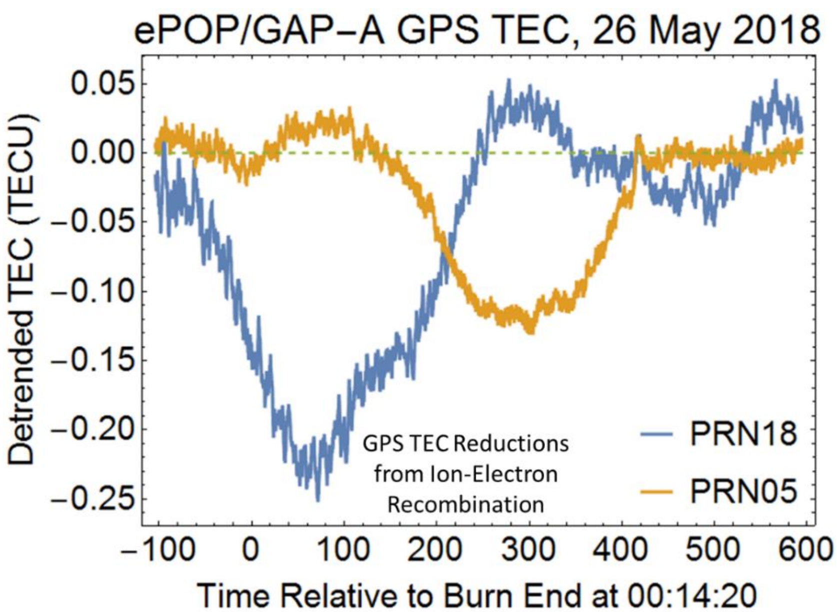

Figure 12. Measured deviations in integrated electron density (TEC) from GPS beacon satellites PRN18 and PRN 05.

The GAP instrument on e-POP serves two purposes for the NG-13 burn experiment. First, the GAP-A (attitude) data register any changes in integrated electron density associated with electron-ion recombination of the molecular ions produced by the charge exchange reactions (2). The recombination process converts the molecular ions into neutrals with the reactions

$$H_2O^+ + e^- \rightarrow OH + H, NO^+ + e^- \rightarrow N + O \qquad (3)$$

as given in numerous papers on the creation of ionospheric holes including Bernhardt [1987]. The GAP-A sensors recorded TEC along 6 separate paths to GPS satellites identified by their PRN number. Two of these paths from PRN18 and PRN05 had TEC changes associated with the Cygnus engine burn (Figure 12).

These data are obtained by subtracting a third-order polynomial fit from the measured TEC over a period of 1000 seconds. The minimum PRN18 and PRN05 TEC are measured 65 and 296 seconds, respectively, after the end of the Cygnus burn. These are interpreted as evidence of molecular ion recombination for Cygnus exhaust charge exchange species.

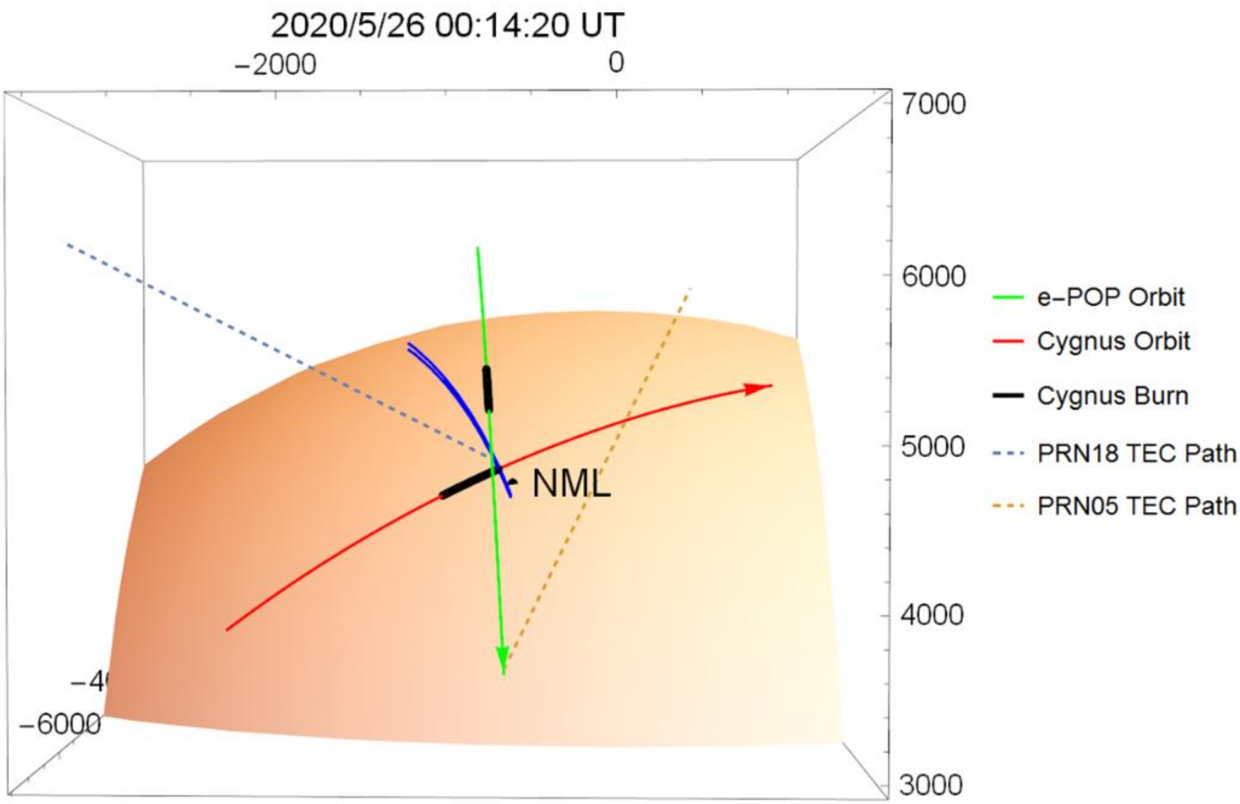

Figure 13. Overhead view of the e-POP/SWARM-E satellite N-S orbit (Green) and Cygnus W-E trajectory (Red) relative to the burn times of the Cygnus BT-4 engine. The dashed lines from GAP to the PRN18 (Blue) and PRN05 (Orange) GPS satellites at times of when a minimum in the GAP TEC measured along the line-of-sight paths. The magnetic field line at the end of the Cygnus burn is shown with a solid blue line.

The time differences in measured TEC reductions are associated with the locations of the GPS satellites relative to the motion of the GAP-A receiver on e-POP. Figure 13 shows the GPS line-of-sight measurement geometry to the GAP sensor relative to the Cygnus and e-POP orbits and locations of the Cygnus burn. The PRN18 path (Dashed-Blue Line) is much closer to the modified field line than the path to PRN05. These measurements of plasma density reductions reinforce the proposition that molecular ions are produced by charge exchange with the Cygnus exhaust followed by electron-ion recombination. This recombination limits the effectiveness of spiraling ions to produce an amplification environment for the whistler mode.

Another, equally important, use of the GAP instrument is to provide electron density profiles with the GPS Occultation technique. The sensor (GAP-O) measures total electron content (TEC) along paths near the limb of the earth. The slant TEC data are processed by an Abel Inversion (AI) technique to determine a profile of the ambient, unmodified ionosphere. This profile compares well with the ionospheric densities from the SAMI3 physics based model and IRI empirical model (Figure 14a). Based on these models, the ion composition and concentration at the Cygnus and e-POP/SWARM-E satellite altitudes are determined to be atomic oxygen ions with a density equal to that of the electrons.

The e-POP MGF instrument provides a magnetic field vector that closely matches the IGRF model of the earth's magnetic field. There is no evidence of any MHD waves seen at frequencies below 40 Hz in the MGF data.

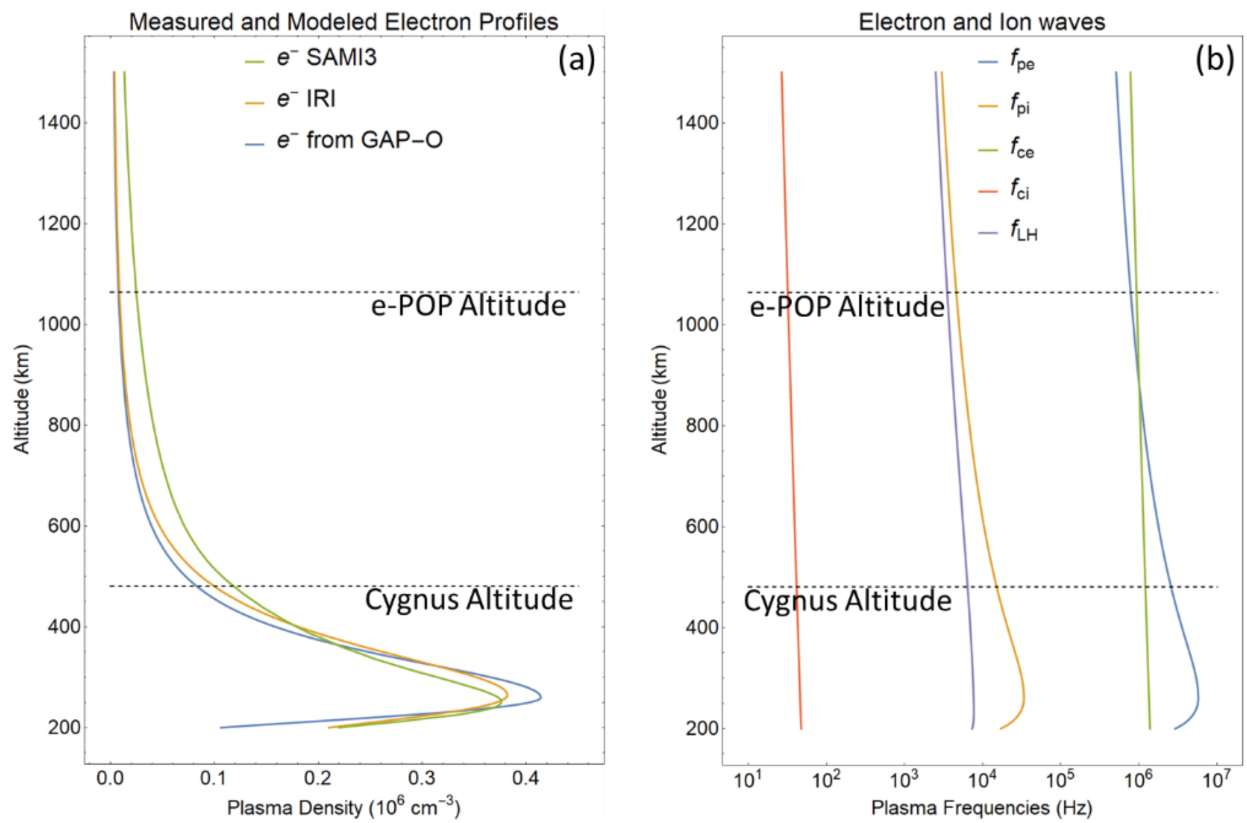

Figure 14. Profiles of (a) electron densities derived from the NRL SAMI3 plasma model, the International Reference Ionosphere Model (IRI), and GPS occultation measurements of TEC and (b) electron and ion plasma frequency, electron and ion cyclotron frequency, and lower-hybrid frequency based on an electron and O^+-ion plasma.

With accurate estimates of plasma density and composition along with magnetic field strength, the plasma frequencies are computed in the ionosphere at the satellite locations (Figure 14b). The electron whistler can be amplified by the Cygnus modified plasma in the frequency range between the ion cyclotron frequency (41 Hz) and the electron cyclotron frequency (1.1 MHz). The frequency cutoff for unducted whistler is the lower hybrid frequency at 6.45 kHz. The electron plasma frequency at Cygnus altitude of 480 km is around 2.6 MHz. The background plasma parameters indicate that the two strongly amplified frequencies, 300 Hz and 25.2 kHz were all whistler modes at both the amplification altitude (480 km) and the receiver altitude (1060 km). The time period for this amplification is labeled VLF and ELF REDA in Figures D and G, respectively.

Based on the magnetic field and electron/ion density models, the relevant plasma frequencies can be determined both at the Cygnus engine injection and at the e-POP RRI sensor altitudes (Table III). The amplified coherent frequencies of 300 Hz and 25.2 kHz are between the ion gyro frequency and the electron gyro frequencies near 40 Hz and 1.2 MHz, respectively. There is no direct coupling between the amplified coherent waves and the lower hybrid frequency of 6.4 kHz. Figures Ca and Cb shows intensification, after the Cygnus engine burn, at the incoherent emissions near lower hybrid (LH) frequency which may be associated with amplification of existing non-ducted whistlers. The other incoherent emission labeled SPWE near 13 kHz was also amplified for a period of about 120 seconds starting 30 seconds after the start of the burn. This emission was attributed to finite k_z lower hybrid waves at the spacecraft [Bernhardt, et al., 2020]. The parameters in Table III should aid future theoretical research to understand the nonlinear amplification processes.

Table III. NG13 Cygnus Experiment Wave Parameters

Plasma Wave Frequency	Cygnus 480 km Altitude	e-POP 1060 km Altitude
Electron Plasma Frequency	2.590 MHz	0.790 MHz
Ion Plasma Frequency	0.151 MHz	0.046 MHz
Electron Gyro Frequency	1.211 MHz	0.936 MHz
Ion Gyro Frequency	41.3 Hz	31.9 Hz
Low Hybrid Frequency	6.41 kHz	3.52 kHz

6. Whistler Mode Propagation in the Magneto-Plasma

The propagation of whistler modes between hemispheres is key to interpreting the RRI data form the Cygnus NG-13 burn. The electron density along a field line determines the path of the electromagnetic whistler waves. With validation provided by the GAP-O plasma profiles shown in Figure 14, the full interhemispheric plasma densities are computed with the SAMI3 model for L shells ranging between L = 2 and 3. The ELF and VLF whistler mode rays are traced with an electromagnetic propagation code written in Mathematica 12 based on numerical solution of by Hamilton's equations

$$\frac{d\mathbf{r}}{d\tau} = \nabla_{\mathbf{k}} H(\mathbf{r},\mathbf{k}), \frac{d\mathbf{k}}{d\tau} = -\nabla_{\mathbf{r}} H(\mathbf{r},\mathbf{k}), \frac{dt}{d\tau} = \frac{dH(\mathbf{r},\mathbf{k})}{d\omega} \qquad (4)$$

for position, directional wave number, and time, respectively. The Hamiltonian is given by

$$H(\mathbf{r},\mathbf{k}) = \frac{1}{2}\left[\frac{c^2}{\omega^2}\mathbf{k}\cdot\mathbf{k} - n^2(\mathbf{r},\mathbf{k},\omega)\right] \qquad (5)$$

where the whistler mode refractive index

$$n^2(\mathbf{r},\mathbf{k},\omega) = 1 - \frac{X(\mathbf{r},\omega)}{1-|\mathbf{Y}\cdot\mathbf{k}|/k} \text{ where } X = \frac{\omega_{pe}^2}{\omega^2}, Y = \frac{\mathbf{\Omega}_{ce}}{\omega}, \omega_{pe}^2 = \frac{e^2 N_e(r)}{m_e \varepsilon_0}, \mathbf{\Omega}_{ce} = \frac{e\mathbf{B}}{m_e} \qquad (6)$$

is a function of the respective plasma and gyro frequencies. The time delay function in (4) leads to the definition of the group-delay refractive index given by $n_g(\mathbf{r},\mathbf{k},\omega) = n(\mathbf{r},\mathbf{k},\omega) + \omega \dfrac{dn(\mathbf{r},\mathbf{k},\omega)}{d\omega}$.

Yeh and Liu [1972], Bernhardt [1979], and Swanson [1989] give further details on the whistler mode ray tracing process.

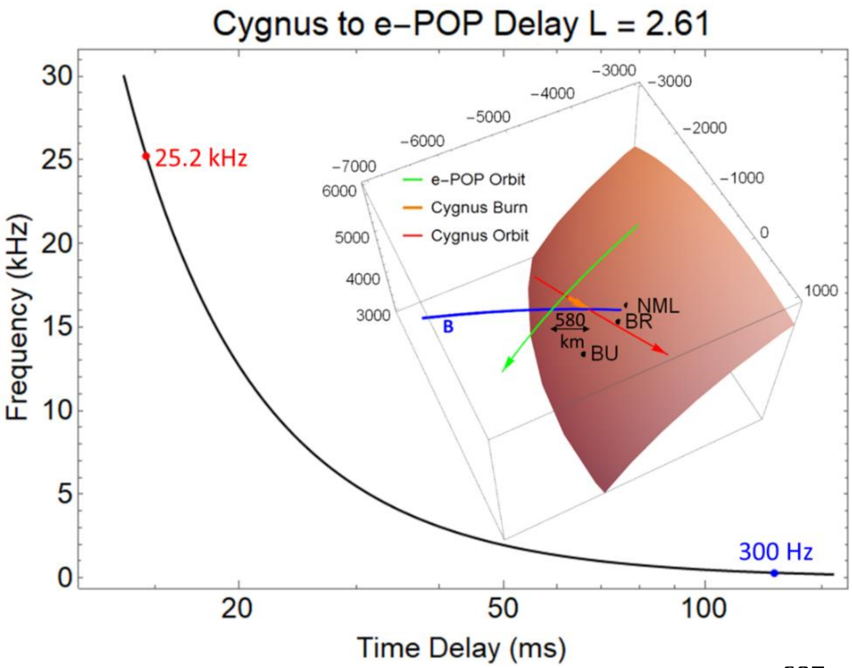

Figure 15. Whistler mode dispersion, with orbit geometry inset, showing time delays along the 580 km path from the Cygnus burn (orange) to the e-POP RRI sensor orbit (green) at the time of closest approach.

The important time delays for the amplified whistler modes are (1) from the amplification region (i.e., around Cygnus) to the receiver (i.e., RRI on e-POP) and (2) from one hemisphere to the other. Computation of the whistler mode propagation requires the magnetic field model based on IGRF and a description of the electron densities along the magnetic field lines. A good estimation of whistler propagation delay is found by integration of the inverse group velocity along the magnetic field line using $t_g = \int_s n_g(\mathbf{r}(s),\mathbf{k},\omega)\dfrac{ds}{c}$ where c is the speed of light. This assumes that the ray path is confined to a magnetic field line and that the wave normal direction is coincident with the direction of **B**.

The calculated propagation times for a whistler excited near Cygnus to be received by RRI on SWARM-E are 127 ms for 300 Hz and 15 ms for 25.2 kHz (Figure 15). The computed whistler group dispersion for inter-hemispheric propagation along the dipole field line is illustrated in Figure 16. The one-hop time delay for 300 Hz is 1.46 seconds and the delay at 25.2 kHz is 0.27 seconds. These times could be resolved with the e-POP RRI with its sample rate at 16 microseconds.

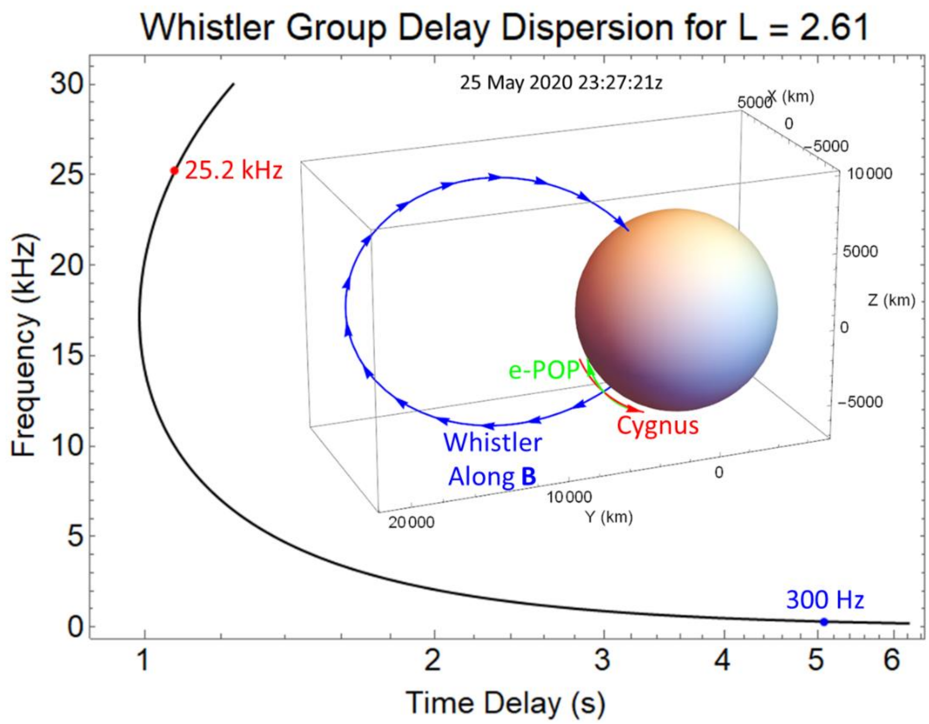

Figure 16. Group delays for amplified whistler mode waves propagating from the Cygnus orbit in the northern hemisphere to the bottom of the conjugate hemisphere ionosphere. The inset shows the magnetic field line associated with guiding the waves for multi-hop propagation.

Raytracing is employed to understand the fate of the amplified waves after they leave the Cygnus exhaust region, couple into VLF field-aligned ducts, and propagate to the conjugate hemisphere. Whistler modewaves can be guided by enhanced columns of plasma along magnetic field lines [Smith et al., 1960, Helliwell, 1965, Angerami, 1970; Bernhardt and Park, 1977; Strangeways, 1981, Rudenchik, 1993]. The gradients at the end of an enhancement duct are critical for determining whether the trapped ray will reflect at or emerge from the endpoint. Thus, a whistler duct acts like a partially reflecting/transmitting mirror for the portions of the trapped EM wave spectrum that echo from and penetrate through the duct end region, respectively. The transmitted wave power propagates downward into the F-region and can be received on the ground. A related duct feature is their capability to capture unducted whistlers at their end points. This feature is critical for exciting ducts with whistler mode waves that eventually interact with radiation belt particles [Burgess and Inan, 2012].

The coupling of whistler waves into VLF ducts has been modeled and explained by Bernhardt and Park [1977]. An example of this coupling for the 300 Hz and 25.2 kHz waves in a duct above the Cygnus amplified region is shown in Figure 17. The many rays for the ELF/VLF waves that have passed through the bottomside ionosphere are refracted to the vertical by the large refractive index of the whistler mode in the plasma. Some of these rays will pass through the rocket exhaust driven amplification (REDA) region and may be captured by an ambient enhancement duct such has been illustrated by the light-blue area in Figure 17. This duct, which extends into the magnetosphere, was created by enhancing the electron density associated with the light ions (H+ and He+) in the SAMI 3 model [Huba and Joyce, 2010; Juba and Krall, 2013] by 8% using the procedure of Bernhardt and Park [1977]. The density enhancement is formed over a region perpendicular to the L = 2.61 magnetic field line with a Gaussian profile width of 0.06 in L. This duct is consistent with observations made by Angerami [1970]. The whistler waves enter this duct from the bottom with wave-normal directions nearly aligned with the earth's magnetic field. The ray paths in Figure 17 are continuous but the nonlinear process in the REDA region may re-radiate plasma waves with **k**-vectors in a spectrum of directions from a parametric amplification process. The observations from the NG-13 Cygnus burn suggest that the amplification process produces a broad wave number spectrum of waves from the source region that can propagate to the RRI sensor at 1064 km and can couple efficiently into ducts above this altitude.

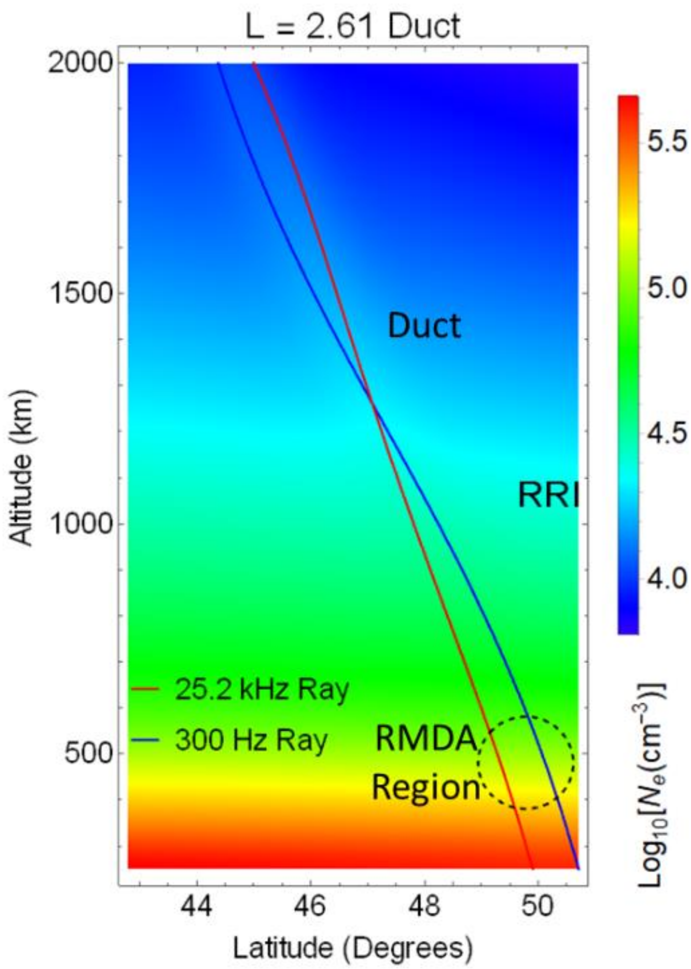

Figure 17. Two ELF (Blue) and VLF (Red) rays from ground sources pass through the F-region and propagate through the REDA region of active ions illustrated in Figure 11. The amplified waves couple into an L = 2.61 enhancement duct extending down from the magnetosphere. Note that the duct is tilted by the magnetic dip angle of 66° and the RRI instrument on e-POP is located slightly to the north of the captured rays.

After an EM whistler is captured by a duct, it can be guided along magnetic field lines by the refractive index gradients across the tube of enhanced plasma. Ducted whistlers with frequencies above one-half the equatorial electron gyro frequency may leak out (i.e., become unducted) and may not reach the conjugate hemisphere [Bernhardt, 1979]. This process is illustrated by the computed ray paths in Figure 18. The electron gyro frequency, f_{ce}, at the equator of the magnetic field line for the Cygnus burn is 47.1 kHz. Thus, a ducted 25.2 kHz signal from NML can follow the magnetic field line until it reaches the equatorial region of the dipole field line where $f_{ce}/2$ is 23.55 kHz and it leaks out [Red curve in Figure 18]. The amplified 25.2 kHz VLF waves are not expected to be ducted across the magnetic equator at L = 2.61 and their 2-hop echoes are not expected to be seen at the e-POP RRI sensor.

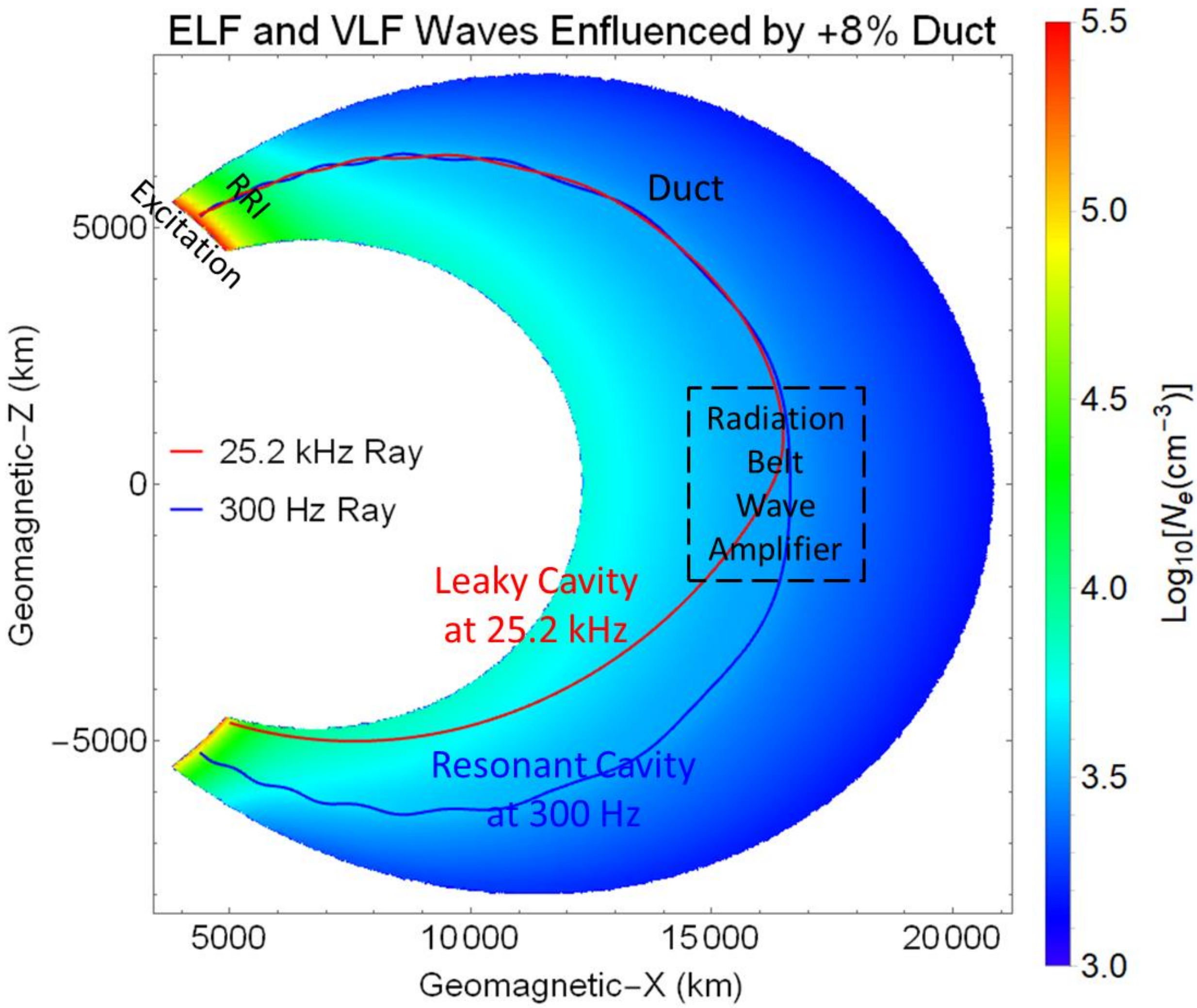

Figure 18. Magnetospherically ducted and partially-ducted whistler mode waves modeled on a field aligned enhancement extending into the protosphere. Both the ELF (blue) and VLF (red) rays are guided by the duct to the equatorial part of the magnetic field line at which point the duct becomes leaky for the VLF wave. The 300 Hz ELF wave remains confined to the duct for either transmission or reflection at the conjugate hemisphere. The ELF wave may be amplified multiple times by this reflection process. The 25.2 kHz VLF wave is amplified only by radiation belts in the cavity.

In contrast, the amplified and trapped 300 Hz signals will be ducted along the magnetic field lines [Blue Curve in Figure 18] to produce multiple-hop echoes that could be observed at the RRI after the burn. The 300 Hz ELF echoes can have amplified interactions with the radiation belt particles on the L = 2.61 magnetic field line and this process may lead to energetic electron precipitation.

The simulated absence of interhemispheric VLF propagation at 25.2 kHz and the much larger amplification of the ELV (300 Hz) signal is consistent with the observations of the amplified signals observed by RRI on e-POP. Figures C through G show that the 20 to 30 dB amplification of the 25.2 kHz VLF waves are only observed for about 23 seconds after the end of the Cygnus burn. In contrast the 300 Hz ELF waves were intensified by 50 dB for at least 180 seconds after termination of the burn [Figure 7]. This long duration effect is attributed to excitation of an active ELF field-aligned resonator established between the two reflection points at the ends of the duct.

We conclude that an echoing whistler train is set up after being initiated with the Cygnus burn amplification of a ground based signal at 300 Hz. This signal excites a VLF whistler mode resonator supported by amplification by cyclotron resonance with radiation belt particles trapped on the magnetic field lines [Figure 18]. The energy of the resonant particles is computed from the cyclotron resonance formula [Sa, 1989; Chang et al., 2014]

$$\frac{\partial \theta}{\partial t} = -k_1 v_{\parallel} - \omega_1 + \omega_{ce} \text{ where } \omega_{ce} = \frac{eB_0}{m_e}, E_{e\parallel} = \frac{1}{2} m_e v_{\parallel}^2 .$$

When particles are in resonance with the whistler wave, the angular velocity $\dot{\theta}$ goes to zero. For the 300 Hz whistler mode amplified by the Cygnus burn, the whistler mode dispersion equation gives k_1 = 0.0000173 m^{-1} and the resonant electron energy is 8.24 MeV which has a flux of 0.1 cm^{-2} s^{-1} sr^{-1} keV^{-1} on an L = 3 magnetic field line as measured with the Van Allen Belt Probes [Zhao et al. 2019a]. The 25.2 kHz whistler has resonance with 21.5 keV electrons which have a flux a million times larger in the L = 3 radiation belts. An optimum choice of frequency for the REDA experiment to induce radiation belt amplification may be in the 2 to 6 kHz range for multiple-hop guiding by field aligned whistler ducts and resonant interactions with large populations of energetic electrons.

Therefore, the REDA process may launch intense whistler waves with additional amplification by the radiation belt environment. The complete system of ground EM transmissions propagating and amplified by the Cygnus burn region with further amplification in the radiation belts is illustrated by the diagram in Figure 19. This same type of process has been used for many years in laser amplifiers with and without an optical cavity [Siegman, 1986]. The whistler mode cavity amplifier is usually excited by lightning with pulse lengths on the order of seconds. Monochromatic waves transmitted from Siple Station, Antarctica have produced 5 dB to 40 dB amplification with growth rates between 20 and 350 dB/s [Li et al., 2014]. Thus it is very reasonable for the radiation belt interactions to produce 20 dB cavity amplification for the long duration ELF (300 Hz) signals as inferred here.

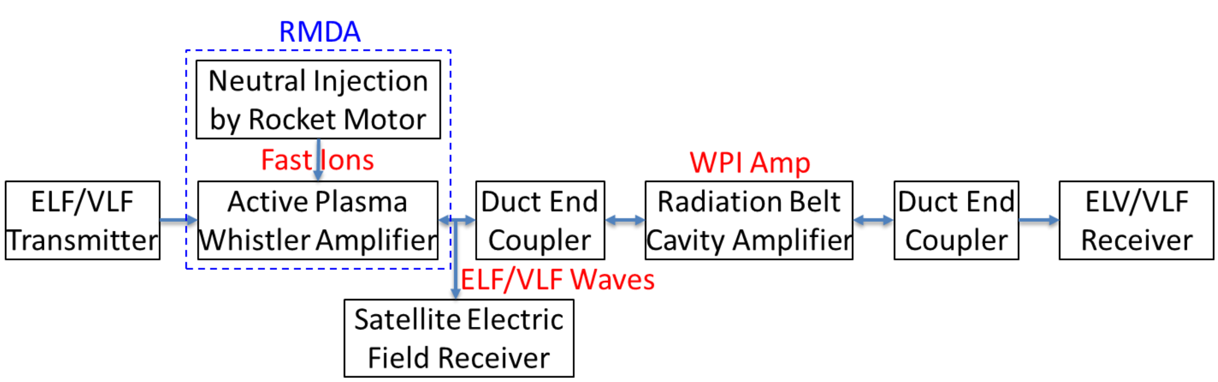

Figure 19. Plasma amplification of whistler mode with cavity excitation. EM waves from the ground VLF transmitters are amplified by the REDA process before they couple into a field aligned duct that acts like a cavity resonator. Leakage from the ends of the ducts should yield ground observable EM waves.

DISTRIBUTION STATEMENT A. Approved for public release: distribution unlimited

7. Summary

Using existing resources in space and on the ground, the first demonstration of rocket exhaust driven amplification (REDA) of whistler mode waves occurred on 26 May 2020. The primary source of coherent VLF waves was the U.S. Navy NML Transmitter at 25.2 kHz located in LaMoure, North Dakota. A region of the topside ionosphere at 480 km altitude became an amplifying medium with a 60 second firing of the Cygnus BT-4 engine. The rocket exhaust, injected as a neutral cloud moved perpendicular to field lines that connected the NML transmitter to the VLF Radio Receiver Instrument (RRI) on e-POP/SWARM-E at 1080 km altitude. The 25.2 kHz VLF signal from NML was amplified by a factor of 10^3 in power (30 dB) for a period 77 seconds as observed with the electric fields measurements by the RRI. A secondary source of coherent ELF waves became amplified by a factor of 10^5 (50 dB) relative to a 300 Hz signal before the engine burn. The 300 Hz ELF waves are of unknown origin but they were related to harmonics of 100 Hz recorded by the RRI more the 600 seconds before the Cygnus burn. Extremely strong coherent emissions and quasi-periodic bursts were observed in the 300 to 310 Hz frequency range for 200 seconds after the release. The actual cavity excitation process may have lasted longer but the orbit of the SWARM-E/e-POP moved the RRI sensor away from the wave emission region. Propagation analysis suggests that the 25.2 kHz VLF waves are less likely to be trapped in plasmaspheric ducts than the 300 Hz ELF band. The longer-lived ELF modes may be the result of multi-hop whistler modes echoing between geomagnetic-conjugate hemispheres.

The primary results of this paper are:

(1) Rocket exhaust driven amplification (REDA) was demonstrated when a Cygnus burn injected hypersonic pickup ions across the propagation paths of ELF and VLF waves. The NG-13 Cygnus Mission found a 0.5% to 25% conversion efficiency for plume kinetic energy conversion into whistler wave energy. Both the nonlinear amplification process and the wave propagation mode determine the electric-field strength at the 580 km range of the receiver. One theory behind this amplification process involves parametrically driven interactions of the narrow-band source waves and lower-hybrid waves. These LH waves are excited by the energetic ion distributions formed when hypersonic neutral flow across the magnetic field lines. Other theoretical mechanisms include conversion of the ring-ion distributions to electron velocity distributions that lead to establishing a broad-band amplifying medium [Lee and Crawford, 1970].

(2) Existing ambient waves in the ELF or VLF frequency range can seed the amplification of low frequency waves produced during chemical injection experiments. The NG-13 SEITE II experiment described here occurred over a known ground source of 25.2 kHz. The ambient 300 Hz waves from an unknown source produced the ELF signals 20 dB larger than the primary VLF source. Any chemical injection or electron beam experiment designed to excite (as opposed amplify) VLF waves should consider these seeding effects. A noise and emission survey in the release region should be made before executing wave generation experiments.

(3) Future REDA experiments will use the electric field instrument in a **Medium or Low Gain Mode**. The NG-13 REDA measurements used the RRI in High-Gain-Mode. As a result, the RRI preamplifier was over-driven by the intensified ELF mode. In addition, modulation of the lower amplitude 25.2 kHz mode by the high amplitude 300 Hz was recorded. Fortunately, analysis has shown that the compression of the 300 Hz and 25.2 kHz carriers of the signals were only 3 and 7 dB, respectively. The **preamp** on RRI has a dynamic range of 120 dB and a gain setting of -11 (low), 19 (medium), and 49 (high). The "hindsight is 20/20" conclusion for the preamp gain is that low or medium gain

levels should have been used to prevent electric field saturation. Since we know that the amplified ELF or VLF signals are around 80 dBμv/Hz, electric field receivers on other satellites can be setup to prevent overloading.

(4) REDA and VLF excitation experiments with the Cygnus BT-4 (and other) rocket motors are being planned for the near future. Several existing satellites with sensitive VLF receivers and energetic particle detectors will be used to detect the amplified waves and their effects in space. Currently, arrangements have been made with the University of Calgary, the Air Force Research Laboratory, and the Institute for Space-Earth Environmental Research at Nagoya University to use wave and particle instruments on the CASSIOPE/SWARM-E/ePOP (Enhanced Polar Outflow Probe), DSX (Demonstration and Science Experiments), and ARASE (Exploration of Energization and Radiation in Geospace) satellites, respectively. Multiple sensor satellites greatly enhance the probability of having an alignment of ground transmitter, the Cygnus burn region and spaced-based VLF receivers near a common magnetic field line. Strong correlations between ground NAA VLF transmissions at 17.8 kHz and >27 keV electron fluxes were observed by Imhof et al. [1983] using the Stimulated Emission of Energetic particles (SEEP) detectors on the S81-1 satellite. The space-based measurements of energetic electron flux enhancements will be much larger after 30 dB amplification of the NAA signal using REDA.

(5) The NG-13 REDA experiment had operational ground receivers recording signals from NML to try to detect Chemical-release-induced electron precipitation (cep) and simultaneous VLF emissions in space and on the ground. This is similar to the detection of lighting-induced electron precipitation (lep) as reported my many authors including Smith, Inan, and Carpenter [1985], Peter and Inan [2007] and Cotts [2011]. A few seconds after the Cygnus burn at 00:13:20, transient VLF phase changes were detected by the UF ELF/VLF receiver system at Chistochina, AK and the GIT VLF/LF receiver at Burden, KS. The phase change was 0.2 degree for about 20 seconds and it is not significant based on signal to noise and in comparison to lightning-inducted electron precipitation (lep) events with 10-degree changes in phase. In addition, NG-13 REDA took place during the day when D-region absorption makes the earth-ionosphere-waveguide insensitive to detection of precipitation events. Future cep experiments will favor Cygnus burns during the night when ionospheric waveguide attenuation is at a minimum.

(6) The REDA technique is relatively inexpensive only requiring coordination and preparation of the Cygnus vehicle for activities after undocking from the Space Station. As such, REDA can be added to any space mission designed to fly devices, such as coherently driven antennas (e.g. DSX) and electron beams (i.e., PIE), on satellites. Future REDA experiments will also be conducted with and without external sources of ELF/VLF waves. The neutral-cloud-injection speed from Cygnus can be increased from 4.2 km/s to 10.5 km/s with a retrograde burn, which adds the spacecraft velocity to the exhaust speed. The added kinetic energy may be sufficient to excite large amplitude VLF waves using the theory proposed by Ganguli [2007].

(7) A critical point of this paper is that theory is not needed as a strong motivator for chemical injection experiments to launch whistler modes for plasma turbulence studies. With the flexibility of the Cygnus-like neutral injections with thruster attitude at any angle between posigrade and retrograde, the injection power can range between 1.3 MW and 8.3 MW. The injection altitude can be chosen between 380 and 480 km to determine impact of collisions and ambient O+ density on the production of pickup ions. For a typical three week period after undocking from the ISS, 5

REDA experiments can be conducted before the end of a Cygnus mission. Supporting theory can be explored after measurements are made.

Acknowledgments. The work at the Naval Research Laboratory was provided under the NRL 6.1 Base Program. Support has been provided to NASA/JSC and Northrup Grumman working with MIT/LL to operate the Cygnus BT4 thruster. The European Space Agency's Third Party Mission Program supports the e-POP instruments on the CASSIOPE/SWARM-E satellite. All data used in this paper is available from the e-POP Data Center at https://epop-data.phys.ucalgary.ca/.

References

Angerami, J.J. (1970), Whistler Duct Properties Deduced from VLF Observations Made with the Ogo 3 Satellite near the Magnetic Equator, J. Geophys. Research Space physics, 75, 6115-6135, 1970

Banks, P.M., and G. Kockarts, **Aeronomy**, Academic Press, 1973.

P. A. Bernhardt and C. G. Park (1977), Protonospheric-Ionospheric Modeling of VLF Ducts, 82, Journal 0f Geophysical Research, 82, 5222-5230.

Bernhardt, P.A. (1979), Theory and analysis of the 'super whistler', J. Geophys. Res., 84, pp. 5131-5142.

Bernhardt, P.A. (1987), A Critical Comparison of Ionospheric Depletion Chemicals, Journal of Geophysical Research, 92, pp 4617-4628, MAY 1, 1987

Bernhardt, P.A., M. P. Sulzer (2004), Incoherent scatter measurements of ring-ion beam distributions produced by space shuttle exhaust injections into the ionosphere, Journal of Geophysical Research, VOL. 109, A02303, doi:10.1029/2002JA009693.

Bernhardt, P.A., J. O. Ballenthin, J. L. Baumgardner, A. Bhatt, I. D. Boyd, J. M. Burt, R. G. Caton, A. Coster,P. J. Erickson, J. D. Huba, G. D. Earle, C. R. Kaplan, J. C. Foster, K. M. Groves, R. A. Haaser, R. A. Heelis, D. E. Hunton, D. L. Hysell, J. H. Klenzing, M. F. Larsen, F. D. Lind, T. R. Pedersen, R. F. Pfaff,R. A. Stoneback, P. A. Roddy, S. P. Rodriquez, G. S. San Antonio, P. W. Schuck, C. L. Siefring, C. A. Selcher, S. M. Smith, E. R. Talaat, J. F. Thomason, R. T. Tsunoda, and R. H. Varney (2012), Ground and Space-Based Measurement of Rocket Engine Burns in the Ionosphere, IEEE Transactions on Plasma Science, 40, 1267.

Bernhardt, P.A., M. K. Griffin, W. C. Bougas, A. D. Howarth, H. G. James, C. L. Siefring and S. J. Briczinski (2020), Satellite Observations of Strong Plasma Wave Emissions with Frequency Shifts Induced by an Engine Burn from the Cygnus Spacecraft, Submitted to Radio Science.

Borovsky JE and Delzanno GL (2019), Active Experiments in Space: The Future, Front. Astron. Space Sci. 6:31, doi:10.3389/fspas.2019.00031

W. C. Burgess, U. S. Inan (2012), The role of ducted whistlers in the precipitation loss and equilibrium flux of radiation belt electrons, Journal of Geophysical Research: Space Physics, 10.1029/93JA01202, 98, A9, (15643-15665).

Carlsten, B.E., P.L. Colestock, G.S. Cunningham, G.L. Delzanno, E.E. Dors, M.A. Holloway, C.A. Jeffery, J.W. Lewellen, Q.R. Marksteiner, D.C. Nguyen, G.D. Reeves, and K.A. Shipman, Radiation-Belt Remediation Using Space-Based Antennas and Electron Beams, IEEE Transactions on Plasma Science, 47, 2045, 2019

Carlsten, B.E. , P.L. Colestock, G.S. Cunningham , G.L. Delzanno, E.E. Dors , M.A. Holloway, C.A. Jeffery, J.W. Lewellen, Q.R. Marksteiner, D.C. Nguyen, G.D. Reeves , and K.A. Shipman, Response to Comment on “Radiation-Belt Remediation Using Space-Based Antennas and Electron Beams” by G. Ganguli and C. Crabtree, IEEE Transactions on Plasma Science, VOL. 48, NO. 2, Feb 2020.

Chang, S.S., S.S. Chang, B.B. Ni, J. Bortnik, C. Zhou, Z.Y. Zhao, J.X. Li, and X.D. Gu, Resonant scattering of energetic electrons in the plasmasphere by monotonic whistler-mode waves artificially generated by ionospheric modification, Ann. Geophys., 32, 507–518, 2014.

Cohen, M. B., and M. Golkowski (2013), 100 days of ELF/VLF generation via HF heating with HAARP, J. Geophys. Res. Space Physics, 118, 6597–6607, doi:10.1002/jgra.50558.1.

Cotts, B.R.T., Global Quantification of Lightning-induced Electron Precipitation Using Very Low Frequency Remote Sensing, PhD Dissertation, Stanford University, 2011.

Ganguli, G., Rudakov, L., Mithaiwala, M. & Papadopoulos, K. Generation and evolution of intense ion cyclotron turbulence by artificial plasma cloud in the magnetosphere. J. Geophys. Res. 112, A06231 (2007).

Ganguli, G., Crabtree, C., Mithaiwala, M., Rudakov, L., and Scales, W. (2015), Evolution of lower hybrid turbulence in the ionosphere. Phys. Plasmas. 22:112904. doi:10.1063/1.4936281

Ganguli, G., Crabtree, C. E., Fletcher, A. C., Rudakov, L., Richardson, A. S., Huba, J., et al. (2019). Understanding and harnessing the dual electrostatic/electromagnetic character of plasma turbulence in the near-earth space environment. Journal of Geophysical Research: Space Physics, 124, https://doi.org/10.1029/2019JA027372.

Ganguli, G. and C. Crabtree, Comment on “Radiation-Belt Remediation Using Space-Based Antennas and Electron Beams” by Carlsten et al., IEEE Transactions on Plasma Science, VOL. 48, NO. 2, February 2020

Gołkowski, M., V, Harid and P, Hosseini, Review of Controlled Excitation of Non-linear Wave-Particle Interactions in the Magnetosphere, Front. Astron. Space Sci., 07 February 2019 https://doi.org/10.3389/fspas.2019.00002.

Hayosh, M., D. L. Pasmanik, A. G. Demekhov, O Santolik, Michel Parrot, et al. (2013). Simultaneous observations of quasi-periodic ELF/VLF wave emissions and electron precipitation by DEMETER satellite: A case study. Journal of Geophysical Research Space Physics, 2013, 118, pp.4523-4533.

Helliwell, R. A, Whistlers and Related Ionospheric Phenomena, Stanford University Press. Stanford. CA. 1965.

R. A. Helliwell, Active very low frequency experiments on the magnetosphere from Siple Station, Antarctica, Phil. Trans. R. Soc. Lond. B. 279, 213-224 (1977).

J. D. Huba and G. Joyce, J. A. Fedder (2000), SAMI2 is Another Model of the Ionosphere (SAMI2)- A new low-latitude ionosphere model , Journal of Geophysical Research, VOL. 105, NO. A10, PAGES 23,035-23,053.

Huba, J.D. and G. Joyce (2010), Global modeling of equatorial plasma bubbles, Geophys. Res. Lett. 37, L17104, doi:10.1029/2010GL044281.

Huba, J.D. and J. Krall (2013), Modeling the plasmasphere with SAMI3, Geophys. Res. Lett. 40, doi:10.1029/2012GL054300.

W. L. Imhof, J. B. Reagan, H. D. Voss, E. E. Gaines, D. W. Datlowe, J. Mobilia, R. A. Helliwell, U. S. Inan, J. Katsufrakis, and R. G. Joiner, “Direct observation of radiation belt electrons precipitated by the controlled injection of VLF signals from a ground-based transmitter,” J. Geophys. Res., vol. 10, no. 4, pp. 361–364, 1983.

James, H.G. (2006) A Digital Radio Receiver for Ionospheric Research. In Characterizing the Ionosphere (pp. 23-1 – 23-16). Meeting Proceedings RTO-MP-IST-056, Paper 23. Neuilly-sur-Seine, France: RTO. Available from: http://www.rto.nato.int/abstracts.asp.

James, H.G., King, E.P., White, A. et al. The e-POP Radio Receiver Instrument on CASSIOPE. Space Sci. Rev. 189, 79–105 (2015). https://doi.org/10.1007/s11214-014-0130-y

C. R. Kaplan and P. A. Bernhardt, “The effect of an altitude-dependent background atmosphere on space shuttle engine burn plumes,” J. Rockets Spacecraft, vol. 47, pp. 700–704, 2010, DOI:10.2514/1.49339.

Kintner, P.M., R. Brittain, M. C. Kelley, D. C. Carpenter, and M. J. Rycroft, In situ measurements of transionospheric VLF waves injection, J. Geophys. Res., 88, 7065, 1983.

Lee, J.C. and F. W. Crawford, Stability Analysis of Whistler Amplification, J. Geophys. Res., Space Phys., 75, 85-96, 1970.

Li, J. D., M. Spasojevic, V. Harid, M. B. Cohen, M. Gołkowski, and U. Inan (2014), Analysis of magnetospheric ELF/VLF wave amplification from the Siple Transmitter experiment, J. Geophys. Res. Space Physics, 119, 1837–1850,doi:10.1002/2013JA019513

Li, X., Y.-L. Huang, G. D. Flesch, and C. Y. Ng (1995), Absolute total cross sections for the ion-molecule reaction $O^+(^4S_o)$ + H_2O, J. Chem. Phys., 102, 5100–5101, doi:10.1063/1.469561.

Ma, Q., Mourenas, D., Li, W., Artemyev, A., & Thorne, R. M. (2017). VLF waves from ground-based transmitters observed by the Van Allen Probes: Statistical model and effects on plasmaspheric electrons. Geophysical Research Letters, 44, 6483–6491. https://doi.org/10.1002/2017GL073885.

Maxworth, A., G. Hussey and M.V. Gołkowski (2020), Coexistence of Lightning Generated Whistlers, Hiss and Lower Hybrid Noise Observed by e-POP (SWARM-E)–RRI, Atmosphere, 11, 177; doi:10.3390/atmos11020177.

Meredith, N. P., Horne, R. B., Clilverd, M. A., & Ross, J. P. J.. (2019), An investigation of VLF transmitter wave power in the inner radiation belt and slot region. Journal of Geophysical Research: Space Physics, 124, 5246–5259. https://doi.org/10.1029/2019JA026715 .

Platov, Y.V., Semenov, A.I. & Filippov, B.P. Condensation of combustion products in the exhaust plumes of rocket engines in the upper atmosphere. Geomagn. Aeron. 51, 550 (2011). https://doi.org/10.1134/S0016793211040153

R. Pradipta, A. Labno, M. C. Lee, W. J. Burke, M. P. Sulzer, J. A. Cohen, L. M. Burton, S. P. Kuo,5 and D. L. Rokusek, Electron precipitation from the inner radiation belt above Arecibo, Geophysical Research Letters, VOL. 34, L08101, doi:10.1029/2007GL029807, 2007

Ross, J. P. J., Meredith, N. P., Glauert, S. A., Horne, R. B., & Clilverd, M. A. (2019). Effects of VLF transmitter waves on the inner belt and slot region. Journal of Geophysical Research: Space Physics, 124, 5260–5277, https://doi.org/10.1029/ 2019JA026716

Parrot, M., Sauvaud, J., Berthelier, J., & Lebreton, J. (2007). First in-situ observations of strong ionospheric perturbations generated by a powerful VLF ground-based transmitter. Geophysical Research Letters, 34, L11111. https://doi.org/10.1029/2007GL029368

Peter, W. B., and U. S. Inan (2007), A quantitative comparison of lightning-induced electron precipitation and VLF signal perturbations, J. Geophys. Res., 112, A12212, doi:10.1029/2006JA012165

Rudenchik, E. A. (1993), Trapping and Propagation of VLF Waves in Ducts: An Analytical Approach, Planet. Space Sci., 41. pp. 619-631.

Sa, L. A. D., A cyclotron resonance mechanism for very-low-frequency whistler-mode sideband wave radiation. I - Introduction and description of external resonances, Journal of Applied Physics, 66, 3482-3514, 1989.

Scherbarth, Mark, Durand Smith, Aaron Adler, Janet Stuart, Greg Ginet, “AFRL's Demonstration and Science Experiments (DSX) mission.” Solar Physics and Space Weather Instrumentation III. Ed. Silvano Fineschi & Judy A. Fennelly. San Diego, CA, USA: SPIE, 2009. 74380B-10. © 2009 SPIE—The International Society for Optical Engineering.

Siegman, A.E., Lasers, University Science Books, 1986.

Smith, A J, Carpenter DL, Inan US, Whistler-triggered VLF noise bursts observed on the DE-1 satellite and simultaneously at Antarctic ground stations, Annales Geophysicae, 3, 81–88, 1985.

Smith, R. L., Helliwell. R. A. and Yahroff (1960), I. W., A theory of whistler in field-aligned columns of enhanced ionization. J. Geophys. Res., 65, 815.

Strangeways, H.J., Trapping of whistler-mode waves in ducts with tapered ends, Journal of Atmospheric and Terrestrial Physics, 10.1016/0021-9169(81)90022-2, 43, 10, (1071-1079), (1981).

Storey, L.R.O., An Investigation of Whistling Atmospherics, Phil. Trans. Roy. Soc. London Ser. A, 246, 113, 1953.

Swanson, D.G., **Plasma Waves**, Academic Press, p. 59, 1989.

Yeh, K.C., and C.H. Liu, Theory of Ionospheric Waves, Academic Press, p. 239, 1972.

Zhao, H., Johnston, W. R., Baker, D. N., Li, X., Ni, B., Jaynes, A. N., et al. (2019a). Characterization and evolution of radiation belt electron energy spectra based on the Van Allen Probes measurements. Journal of Geophysical Research: Space Physics, 124, 4217–4232. https://doi.org/10.1029/2019JA026697

Zhao, S., Zhou, C., Shen, X. H., & Zhima, Z. (2019b). Investigation of VLF transmitter signals in the ionosphere by ZH-1 observations and full-wave simulation. Journal of Geophysical Research: Space Physics,124,4697–4709. https://doi.org/10.1029/2019JA026593

Záhlava, J., Němec, F., Pincon, J. L., Santolík, O., Kolmašová, I., & Parrot, M. (2018). Whistler influence on the overall very low frequency wave intensity in the upper ionosphere. Journal of Geophysical Research: Space Physics, 123, 5648–5660. https://doi.org/10.1029/2017JA025137